Summer 8-18-2023

# Impact of Solar Generation on IEEE 9-bus System

Tasnim Ikra Rahman
*University of Maine*, tasnim.rahman@maine.edu

# IMPACT OF SOLAR GENERATION ON IEEE 9-BUS SYSTEM

By

Tasnim Ikra Rahman

BSc, Military Institute of Science and Technology, Bangladesh, 2016

MS, University of Dhaka, 2019

A THESIS

Submitted in Partial Fulfillment of the

Requirements for the Degree of

Master of Science

(in Electrical Engineering)

The Graduate School

The University of Maine

August 2023

Advisory Committee:

Mohamad Musavi, Professor of Electrical and Computer Engineering,

Associate Dean of College of Engineering, Advisor

Yifeng Zhu, Professor of Electrical and Computer Engineering

Paul Villeneuve, Professor of Electrical Engineering Technology

Shengen Chen, Senior Power System Engineer at RLC Engineering

Jonathan Gay, Principal Power System Engineer at RLC Engineering

# IMPACT OF SOLAR GENERATION ON IEEE 9-BUS SYSTEM

By Tasnim Ikra Rahman

Thesis Advisor: Dr. Mohamad Musavi

An Abstract of the Thesis Presented
in Partial Fulfillment of the Requirements for the
Degree of Master of Science
(in Electrical Engineering)
August 2023

There has been an increasing interest in renewable energies due to public awareness of the negative effects of fossil fuel-fired electricity generation on the environment, and policies have been enacted requiring progressive reduction of such generation. Due to some favorable characteristics of solar over other renewables, solar power has grown considerably.

Integration of solar generation into the existing power grids poses significant challenges. Solar generators' limited reactive power capability can cause several problems, such as significant voltage drops or rises in the system. Therefore, voltage stability is a major concern. This thesis presents an investigation of the voltage characteristics of an electric microgrid connected to solar generators and subject to increasing penetration of solar generation.

The New England region possesses abundant potential for developing microgrid power generation. However, microgrids are installed mostly in remote locations in Northern New England, far from major load centers. Therefore, long transmission lines are required to connect the microgrids to the rest of the power grid. This study includes an analysis of the level of renewable energy penetration into the grid while keeping the system stable. The voltage magnitude, angle, and losses seen by the system have been used as a measure of stability. The test case system used in this thesis has not been used in the literature review for analyzing the stability,

and it is proved by this work to be a useful tool for assessing the best option when connecting a solar farm to a power grid.

The IEEE standard 9-bus system, a simplified representation of an electric grid, has been used to illustrate the developed methodology. The present study has set the basis for extending the analysis to the real New England power system.

## DEDICATION

To my parents and sisters.

## ACKNOWLEDGEMENTS

Foremost, I would like to extend sincere gratitude to my incredibly amazing advisor Dr. Mohamad Musavi, for his unparalleled support, guidance, motivation, and mentorship. His continuous academic and moral support, encouragement, and patience have made it possible for me to complete this thesis. I honestly count myself fortunate to have worked with him and cannot ever thank him enough for teaching me, training me as a researcher, and making my graduate experience enjoyable and truly rewarding. I would also like to thank my committee members- Dr. Shengen Chen, Paul Villeneuve, Jon Gay, and Dr. Yifeng Zhu for their invaluable feedback and guidance. They have devoted their time and provided me with helpful suggestions to improve my research.

It has been an absolute privilege for me to be a part of the Department of Electrical and Computer Engineering — the most supportive and inspiring team. I have developed both professionally and personally while working with my professors and classmates. I also extend my thanks to the Office of International Programs and my friends in Orono, who have turned Maine into a second home for me.

My parents and sisters have always been there for me not only during this journey but throughout my life. I thank the Almighty for blessing me with such a supportive, loving, and caring family, and I will remain forever grateful to my family for their unconditional support and belief in myself.

## TABLE OF CONTENTS

## LIST OF TABLES

## LIST OF FIGURES

# CHAPTER 1

# INTRODUCTION

This chapter serves as an introduction to the work developed in this thesis. The motivation for conducting this research, along with its objective and the approach taken, are explained. The organization of the rest chapters of the thesis is included at the end of this chapter.

## 1.1. Motivation and Background

First, the motivation for developing this work will be explained, summarizing the enormous potential of solar energy but also the challenges that it poses to power systems. These challenges are motivating major research in the area of solar power, given its many advantages.

### 1.1.1 Solar Energy Opportunities and Challenges

There has been increasing interest in renewable energies due to public awareness of the negative effects on the environment of fossil fuel-fired electricity generation resources. The United States has enacted renewable energy mandates that require utilities to utilize a certain percentage of electricity from renewable sources. Usually, the required percentage of renewable electricity increases over time until reaching a target percentage, such as 20% or 25%, at a target year, such as 2020 or 2025. Twenty-nine states have renewable electricity mandates, and an additional six states have renewable electricity goals [1]. Due to some favorable characteristics of solar over other renewables, solar generation has grown considerably in the last two decades [2].

The New England region, which comprises six states in the northeastern corner of the US, possesses abundant potential for developing microgrid power generation. A microgrid can be defined as a group of distributed energy resources that can provide power either in grid-connected or in islanded mode. The reason why microgrids are becoming popular nowadays is that they can

provide energy with high efficiency and reasonable cost features. A microgrid is usually a small-scale power system with small power generation units. Around four hundred microgrids are currently in operation across the United States, and this accounts for 0.2% of the US total generation. Generation capacity for all the microgrids working is estimated at 3.1 gigawatts. However, there are some concerns about the stability, power quality, cost, and efficiency of those microgrids [3]. There were 24,645 electric generators at about 11,925 utility-scale electric power plants in the United States calculated in 2021. The average generation capacity for utility power plants is one megawatt. Microgrids can produce around 100 kilowatts to multiple megawatts [4-6]. Renewable energy sources are also an important part of producing electricity. The percentage of renewable sources in 2021 is about 20% in total, where wind energy contribution is about 9.2%, 6.3% for hydro, 2.8% for solar, 1.3% for biomass, and 0.4% for geothermal energy. Conventional sources contain 19% nuclear, 22% coal, and 38% natural gas, as shown in Figure 1.1.

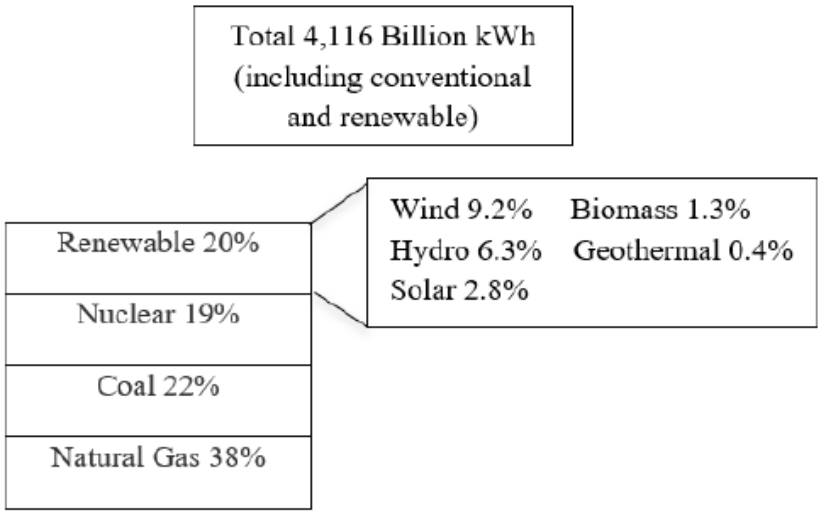


Figure 1.1 US electricity generation, 2021 [3]

As opposed to other generation resources like nuclear or gas, whose location may be chosen by system planners, the location of microgrids is selected primarily based on good geographical conditions, although it is also subject to environmental and economic constraints [7].

As summarized in the previous paragraphs, solar generation has great potential, particularly in the New England region. However, integrating solar generation into the existing grid poses some significant challenges from the electrical point of view, particularly due to the limited reactive power capability that solar plants have. This can cause several voltage problems, such as significant voltage drops or rises and fluctuations at the point of connection with the rest of the power grid [8-9]. Although modern solar farms include power electronic converters with reactive power regulation capability that allows certain control over voltage disturbances, the capacity of the power electronics is limited [10]. When a contingency occurs in the system, the inability of solar farms to provide enough reactive power so that the voltage can go back to its pre-fault value is a major concern. Therefore, dynamic voltage stability, which is defined as the ability of a power system to maintain steady voltages at all buses after a disturbance, is one of the biggest issues regarding solar integration. It should also be pointed out that it is essential to take into account the distinctive features of solar power, such as its usually remote geographical location, when conducting solar integration studies.

Typical solar generation project proposals assume a basic configuration, which must include solar generators as part of the system. System Impact Studies (SIS) often identify additional system elements needed to ensure that the proposed generation does not degrade the power system performance. These additional system condition installations often appear as significant economic burdens. The present study focuses on analyzing basic solar installations in

microgrids to identify the appropriate actions that should be taken to improve their voltage performance.

### 1.1.2 Analysis of Existing Literature

As mentioned in Section 1.1.1, stability is one of the biggest concerns when conducting solar integration studies connected with microgrids. Microgrid technology has become popular in the last decade as it has many advantages over conventional power grids. The most interesting feature is that microgrids can be used both in grid connected and in islanded mode. In grid connected microgrids, normally all generators are connected in a local network, and they are tied to the main grid via a substation or one of the sources. Whereas, in island mode, all sources will be independently working [5].

The microgrid concept provides the scope to increase distributed generation and produces output with cost-effectiveness and environmental protection. A microgrid is the most accepted and reasonable option if conventional grids must be replaced. Generation and demand side management in case of having critical loads and maintaining power quality better than conventional systems are other benefits that we can get from microgrid installation. For successful Distributed Energy Resources (DER) integration, proper operation and control, protection, and stability need to be established. Policy management is also needed, which can vary from country to country. Also, economic and financial benefits are facts associated with this generation technique. Climate change and safety measures for energy are other reasons for increasing installment of renewable energy sources and distributed generation. Most of the states in the US are considering installing renewable sources as an alternative. It can be used as a key to future energy storage security as the dependency on conventional sources will be reduced. Also, using microgrids with distributed sources can solve the financial problems [11].

As microgrids can operate in both grid connected and islanded mode, where grid dependency on end users is less. Microgrids are also more energy efficient and cost-effective as they can reduce fuel consumption while using renewable sources. Operating cost is also lower than conventional power generation techniques if distributed resources are used. Furthermore, microgrids increase reliability by using battery storage which can ensure the availability of reserve power. So, microgrid systems will be more efficient while also improving power quality [12].

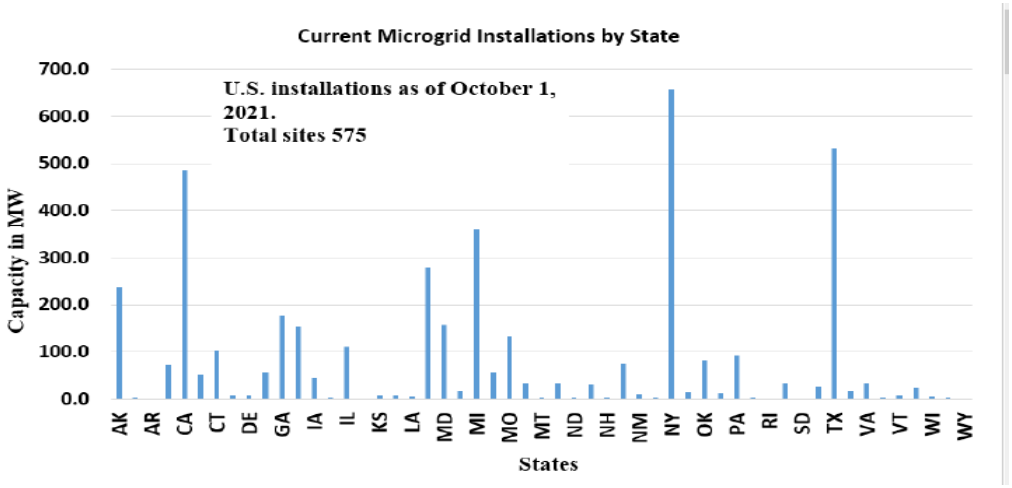


Figure 1.2 Current microgrid installation by states [3]

Using microgrids can provide many advantages over the conventional power system which include simplification or modernization of grid technologies, improving operation and stability of the regional electric grid, increasing reliability and resilience, and applying smart grid technologies. Economic study on microgrids at Yuma/AZ/USA, Boston/MA/USA, Ma'an/Jordan, and Plymouth/England showed that renewable energy systems within the microgrids reduced the Net Present Cost (NPC) of the conventional microgrid up to 44% [3]. Advanced technology in power system analysis includes installing microgrid technologies. Renewable energy Technologies (RET) like solar, wind, hydro, and biomass are used widely in modern power

systems. Integration of RET in microgrids and how this is being utilized in modernization is shown in Figure 1.3.

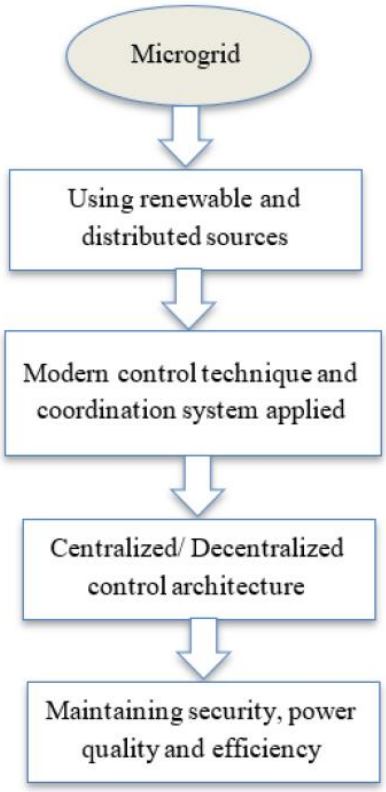


Figure 1.3 Power system modernization flow chart [3]

There are hundreds of microgrid projects running in the US. Among them, the majority of microgrids are connected to distributed generations like solar, wind, hydro, and other sources. As of 2021, there are a total of 575 active sites using microgrids producing 4256 MW of energy [3]. The major issues related to microgrids include the size difference of microgrids compared with the regular power systems, high penetration of renewable energy resources, unbalanced loading for three phases, lower short circuit capacity, etc [9-10]. For ideal operation, microgrids need to maintain certain parameters which includes defined range of voltages, currents, frequency,

maintaining balance between power supply and demand, and economic dispatch. The control and coordination systems are different as microgrids provide different characteristics in terms of dynamic performance, numerical and mathematical relationships between voltages, angles, active and reactive power flows. For high penetration of power electronic switches and nonlinear loads in microgrids, power quality drops and it has a negative impact on the stability of the overall system. Distributed resources are also responsible for dropping power quality in microgrids when penetration level is high. That means the sinusoidal voltage and frequency rate cannot be maintained at the buses at the time of disturbance.

Studies on the impact of solar generation on microgrids are available but there is still a need to identify how microgrids work when the penetration level increases under different conditions. However, there might be alternative solutions to the problem of poor dynamic voltage performance of basic solar installations, which may be simpler and/or more cost-effective. Many of these studies use the Short Circuit Ratio, a magnitude related to the Thevenin impedance equivalent of the grid, as a measure of the strength of the interconnection.

As a conclusion for this literature review, it should be pointed out that there is a need for research focusing on the voltage behavior of solar farms while taking into consideration the long transmission lines that connect them to the rest of the power grid. Furthermore, solar farms need to be further studied for transient analysis, given their projected increase in market share and the scarce literature currently available.

### 1.2 Research Objective

The aim of the present thesis is to analyze the voltage characteristics of an electric microgrid connected to solar generation and subject to increasing levels of renewable penetration.

Given the continuous increase of solar power in the world, the need for studies such as this one has become critical in order to maintain power quality and stability. Grid-connected microgrids are studied, with the goal of expanding the current knowledge of stability performance and shedding light on the impact of high solar installation at a particular bus of the system. The ultimate objective of conducting such a study is to be able to identify appropriate actions that can remediate the voltage problems caused by solar generation. While this is an academic study, its practical application has always been in the spotlight of researchers. The typically remote location of solar resources, particularly in the New England region, makes it necessary to use long transmission/distribution lines to connect solar farms to the rest of the power system [13]. That is why studying the effects of such an electrical connection on voltage performance is one of the cornerstones of this work [14-15].

### 1.3 Research Approach

In order to achieve the goal of quantifying the impact of solar power on voltage performance of a power grid, several simulations have been conducted. The IEEE standard 9-bus system, which is a simplified representation of an electric grid, has been used as a platform to show the result of the study. The software used to conduct the simulations is SKM and Power System Analysis Toolbox (PSAT) for MATLAB. Both are research-oriented software that give the user great flexibility and the ability to easy prototype when compared to commercial tools.

First, the performance of grid-connected microgrids has been compared under different load conditions. Simulations have been conducted considering synchronous machines connected to some of the IEEE 9-bus system and solar generation connected to bus 6 of the grid in order to study the impact of increased solar generation on voltage profiles [16-18]. In addition, several solar penetration scenarios have been considered. These cases have been simulated under different

conditions in the system. The losses for both active and reactive power seen by the solar bus have been used to measure the strength of the point of interconnection.

### 1.4 Thesis Organization

The organization of the remaining Chapters of this thesis can be summarized as follows.

Chapter 2 discusses the models of different power system elements and devices used in this study, such as synchronous generators, solar generator specifications, and transmission lines. An explanation of the automated simulation process is also included in this Chapter.

Chapter 3 deals with the grid-connected microgrid, with different performances of solar generators connected at bus 6 and synchronous generators regarding system voltages. Several solar integration scenarios are considered in order to quantify the impact of increasing solar power in the network.

In Chapter 4, the conclusion of the results has been discussed, and the limitations of this study have been discussed.

# CHAPTER 2
# POWER SYSTEM MODELLING AND SIMULATION

This Chapter discusses the models of the different power system elements and devices used in this study, such as synchronous generators, solar generators, and transmission lines. An explanation of the automated simulation process and analysis of results that has been developed for this thesis is also included at the end of this Chapter.

## 2.1 Simulation Tool: SKM's Power Tools for Windows

The software used to conduct the simulations is SKM. SKM Power Tools software is used to accurately simulate real events that occur in an electrical power network to easily understand the dynamics of any changes made to the network [19]. SKM is an open-source power system analysis toolbox that can be used for power system analysis and control learning, education, and research. It is a research-oriented software that gives the user more flexibility and the ability of easy prototyping compared to commercial tools, which are focused on achieving computational efficiency. In addition, SKM has been used for several renewable integration studies [20]. One of the reasons for its use in solar power analysis is the solar generator models that SKM includes, which are based on the models developed in [21], particularly created for conducting load flow analysis. Furthermore, the solar generator models implemented in SKM are adequate for representing a single microgrid as well as a whole grid composed of several generators.

On the other hand, SKM has some limitations. As mentioned before, it strengthens flexibility for the user in detriment to computational efficiency, which makes it unsuitable for studying real power systems containing thousands of buses. However, this thesis is an academic work that uses IEEE 9-bus system instead of a real power grid as the platform to conduct the study. The 9-bus test case has been chosen due to its numerous advantages when used for research work,

which will be discussed in Section 2.2. Therefore, SKM is a perfectly valid simulation package for the present work.

As with most power system simulation packages, SKM uses the single-phase equivalent representation of a power system. This is an acceptable representation when three-phase balanced magnitudes are considered all over the power system, as is assumed in this thesis.

In the following Sections, the models of the devices of interest for the present study will be discussed. For a detailed description of the rest of the models of power system elements included in SKM, please refer to [22]. A brief description of the physical fundamentals of each of the devices is also included in the following Sections.

### 2.1.1 Synchronous Generator Model

Large-scale power is mainly generated by three-phase synchronous generators, which are the traditional type of generators driven by steam, hydro or gas turbines in all the conventional power generation facilities before the rise of renewables. The synchronous generator has two main components: the stator and the rotor. The stator contains armature windings, which are designed to generate balanced three-phase voltages. The rotor contains field windings, and its function is to induce voltages in the stator winding by means of a rotating magnetic field. For this magnetic field to be created, a DC excitation system is used to inject a direct current into the rotor's windings. Moreover, the rotor constantly rotates because it is connected to the already-mentioned steam, hydro, or gas turbine, and this rotation makes the magnetic field change over time [23].

The synchronous machine model used in SKM simulations in this thesis represents a synchronous machine, which corresponds to the classic electro-mechanical model, used for

deducing the classical swing equations in the literature [24]. This model considers a constant amplitude excitation voltage of the rotor windings.

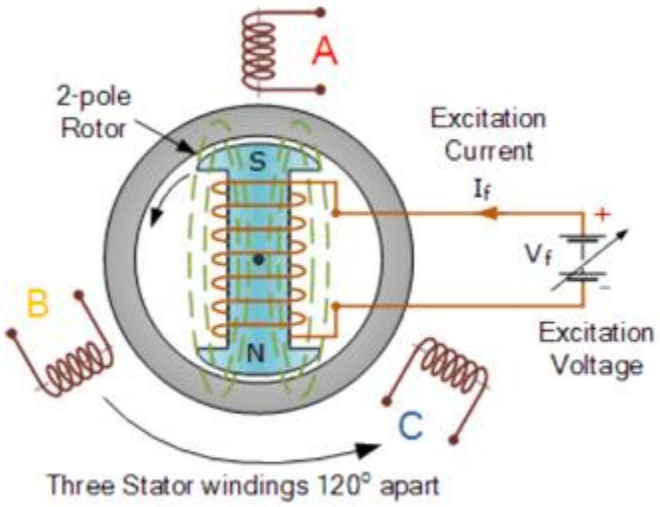


(a)

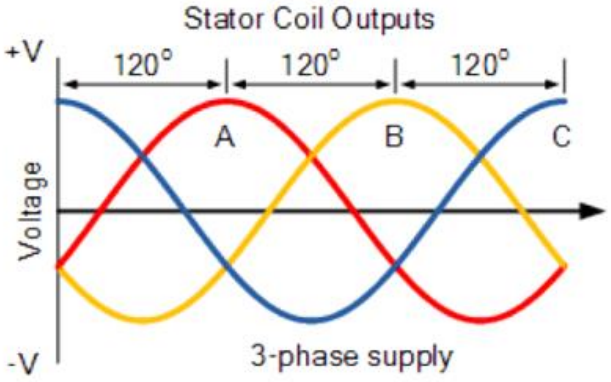


(b)

Figure 2.1 (a) Schematic of a three-phase synchronous generator (b) Three-phase output [25]

### 2.1.2 Solar Generator Model

In this study, the photovoltaic system considers the built-in Photovoltaic model in the SKM software. The PV generation systems are modeled through the solar generator block, shown in Figure 2.2 (a) [26]. The photovoltaic model is based on an equivalent circuit with a single diode shown in Figure 2.2 (b).

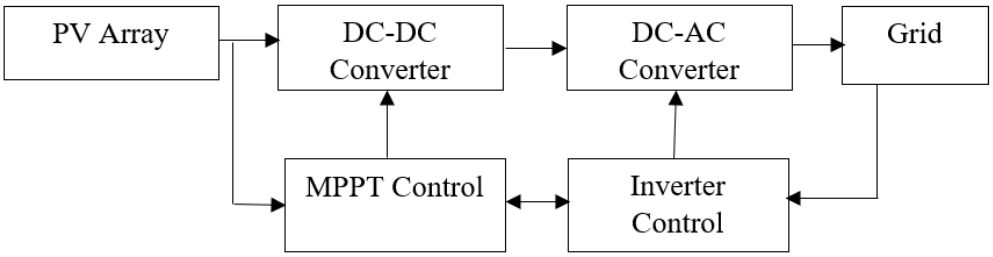


(a)

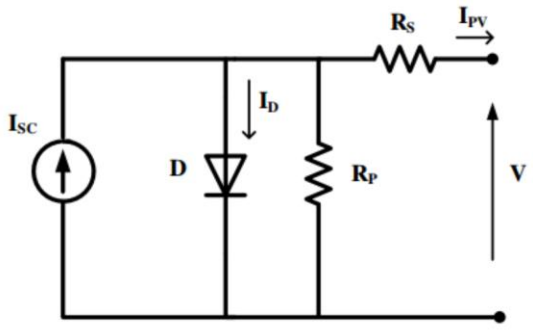


(b)

Figure 2.2 (a) Block diagram of PV system (b) PV cell equivalent circuit [26]

With the variation of cell temperature and irradiation (the output of light energy from the sun), there will be a considerable change in voltage and current, which result in the increase or decrease of PV cell power output described in Equation 2.1.

$$P_{pv}(t) = Npv \,.\, Voc(t) \,.\, Isc(t) \tag{2.1}$$

Where,

$$I_{SC}(t) = [\, I_{SC,STC} + K_i [T_c(t) - T_{ref}(t)\,] \frac{G(t)}{1000} \quad (2.2)$$

$$V_{OC}(t) = V_{OC,STC} + K_v [T_C(t) - T_{ref}(t)] \quad (2.3)$$

The solar operating temperature $T_c$

$$Tc(t) = T_A(t) + \frac{NCOT-20}{800} G(t) \quad (2.4)$$

Where,

$N_{PV}$: Number of PV modules

$V_{OC}$: Open circuit voltage

$I_{SC}$: Short circuit current

STC: Standard test condition

$K_i$: Short circuit current coefficient

$T_{ref}$: Reference operating condition (25°C)

G: Solar irradiance

Kv: Open circuit voltage coefficient

TA: Ambient temp

NOCT: Nominal operating cell temperature.

Reactive power is the power that is used to establish and maintain the magnetic field in inductive loads such as motors, transformers, and fluorescent lights. It does not perform any work in the electrical system but is necessary to maintain voltage levels and ensure the proper functioning of the equipment.

Solar PV generators typically inject reactive power into the electrical system in addition to real power. The amount of reactive power injection depends on the type and configuration of the PV inverter used in the system. Inverters can be designed to inject reactive power in two ways:

either as a fixed amount, which is predetermined by the inverter design or as a variable amount, which is determined by the operating point of the inverter.

The reactive power injection from the solar PV generator can cause the voltage at the bus where the PV generator is connected to rise. This happens because reactive power injection results in a flow of current that lags behind the voltage, creating a voltage drop across the impedance of the distribution lines. This voltage drop can be significant when the system is heavily loaded, causing the voltage at the bus to rise.

**Variable Reactive Power Injection**:

Inverters can also be designed to inject variable amounts of reactive power into the system, which are determined by the operating point of the inverter. The amount of reactive power injection is controlled by adjusting the inverter's voltage magnitude and phase angle, which can be achieved through various control strategies such as voltage control or droop control.

The mathematical formula for calculating the reactive power injection for a variable power factor angle ($\theta$) is:

$$Q = P \times \tan(\cos^{-1}(PF) - \theta) \quad (2.5)$$

Where:

Q = Reactive power injected by the inverter (VAR)

P = Real power output of the inverter (W)

PF = Power factor of the inverter ($\cos(\theta)$)

$\theta$ = Power factor angle (degrees) of solar generator

### 2.1.3 Transmission Line Model

It is convenient to represent a balanced three-phase transmission line by the two-port pi-equivalent network shown in Figure 2.3, where $VS$ and $IS$ Is are the sending-end voltage and current and $VR$ and $IR$ are the receiving-end voltage and current [15]. This lumped equivalent model of a transmission line is an acceptable representation for most studies, and it is the model implemented in the SKM software. The magnitudes Z and Y are usually calculated by multiplying the line per-length impedance *z* and per-length admittance *y* by the total line length, respectively.

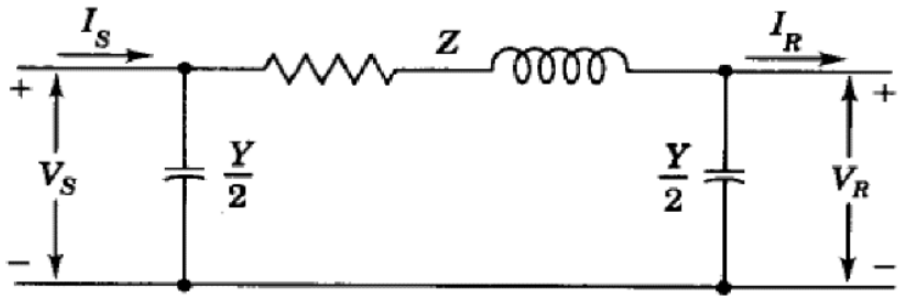


Figure 2.3 π-nominal model of a transmission line [15]

The values for transmission line impedances are listed in Table 2.2.

### 2.2 IEEE 9-Bus Test Case

The platform used to conduct this study is the IEEE standard 9-bus system, which represents a microgrid representing a greatly reduced model of an electric grid. The 9-bus system is a standard system for testing new methods, which has been used by numerous researchers to study both static and dynamic problems in power systems. Using test systems is considered more convenient than using models of real power systems, as the latter is not fully documented and tend to be very big, which makes it difficult to distinguish general trends. Furthermore, the results obtained with models of real systems are less generic than those obtained with test systems [30].

The IEEE 9-bus system has 3 generators, 3 loads, 10 transmission lines and 3 transformers, as shown in Figure 2.4.

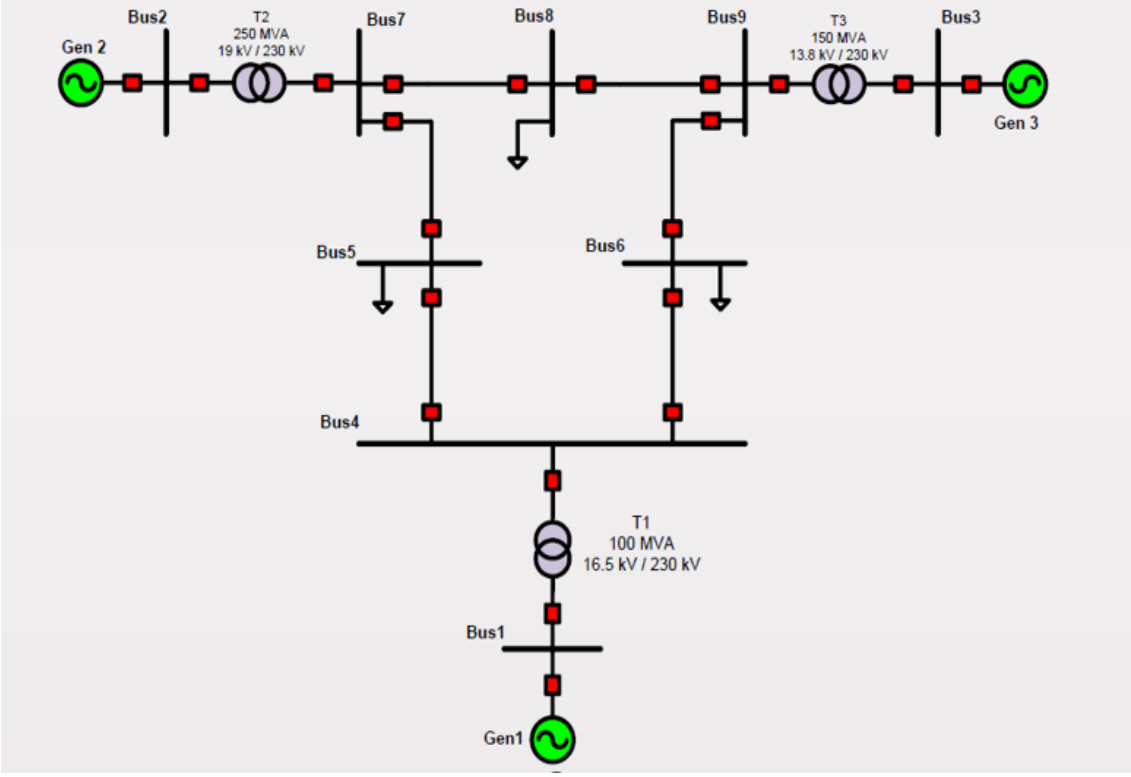


Figure 2.4 Diagram of the IEEE 9-bus system [31]

### 2.2.1 IEEE 9-Bus Case Data

The input bus and transmission line data are listed in Table 2.1 and Table 2.2 [31]. These values have been used throughout the research. Six scenarios have been analyzed in this thesis, so some values have been changed according to the case study.

The bus data, branch impedance values, and transmission line data given for the IEEE 9-bus system are listed in Table 2.1 and Table 2.2. For different cases considered in this thesis, some values have been modified from the original ones. The changed values have been listed in the

respective section for each scenario. Throughout this research, the loads and transmission line values have not been changed.

Table 2.1 Bus Data of IEEE 9-bus system [31]

| Bus No. | Bus Code | Voltage (P.U.) | Generation | | Load | |
|---|---|---|---|---|---|---|
| | | | MW | MVAR | MW | MVAR |
| 1 | 3 (Slack) | 1.04 | 0 | 0 | 0 | 0 |
| 2 | 2 (PV) | 1.025 | 163 | 6.7 | 0 | 0 |
| 3 | 2 (PV) | 1.025 | 85 | -10.9 | 0 | 0 |
| 4 | 1 (PQ) | 1 | 0 | 0 | 0 | 0 |
| 5 | 1 (PQ) | 1 | 0 | 0 | 125 | 50 |
| 6 | 1 (PQ) | 1 | 0 | 0 | 90 | 30 |
| 7 | 1 (PQ) | 1 | 0 | 0 | 0 | 0 |
| 8 | 1 (PQ) | 1 | 0 | 0 | 100 | 35 |
| 9 | 1 (PQ) | 1 | 0 | 0 | 0 | 0 |

For analysis explained in chapter 3, utility connected has been considered as a slack bus as the system is using a grid connected microgrid. Table 2.1 shows the original data where bus 1 is used as a slack bus. Also, MVAR values of loads have been considered as zero for analysis purposes. Table 2.2 shows the branch data of IEEE 9-bus system.

Table 2.2 Line or Branch Data of IEEE 9-bus System

| Line From | Line To | R | X | ½\|Y\| | Y |
|---|---|---|---|---|---|
| 1 | 4 | 0 | 0.0576 | 0 | 0 |
| 4 | 5 | 0.01 | 0.085 | 0.088 | 0.176 |
| 4 | 6 | 0.017 | 0.092 | 0.079 | 0.158 |
| 6 | 9 | 0.039 | 0.17 | 0.179 | 0.358 |
| 5 | 7 | 0.032 | 0.161 | 0.153 | 0.306 |
| 9 | 3 | 0 | 0.0586 | 0 | 0 |
| 7 | 2 | 0 | 0.0625 | 0 | 0 |
| 9 | 8 | 0.0119 | 0.1008 | 0.1045 | 0.209 |
| 7 | 8 | 0.0085 | 0.072 | 0.0745 | 0.149 |

## 2.3 Automated Simulation and Analysis

The impact of solar power on the voltage performance of the IEEE 9-bus system is studied in this thesis through simulations in SKM. These simulations are widely used to study the behavior of power systems under contingencies. This kind of simulation includes dynamic models of the power system's elements and devices, which are described by nonlinear equations. The differential equations are solved by computer simulation packages using numerical methods, which use different techniques to improve the efficiency of the simulation while converging to an acceptable solution for the dynamics of the system.

One of the contributions of this thesis is, in fact, the model developed for automating the simulations and the analysis of its results, as it will be available to future students conducting power system analysis with SKM or ETAP. ETAP (Electrical Transient and Analysis Program) is

used for simulation and design of industrial power systems. These results could potentially be included in the software library as an additional functionality of the toolbox, so that all its users can benefit from it, therefore contributing to the philosophy of open-source freeware as PSAT toolbox in MATLAB.

### 2.4 Load Flow Analysis in SKM

A load flow study is done on a power system test-case and several parameters such as voltage magnitude at buses, angles, slack bus real and reactive power, and system losses have been monitored [27-29]. A Load Flow Study specifically investigates bus voltages, the effect of injecting in-phase and quadrature boost voltages on system loading, optimum system running conditions and load distribution, optimum system losses, optimum rating and tap range of transformers. The basic equation for power-flow analysis is derived from the nodal analysis equations for the power system. For example, for a 3-bus system, the equations are presented by:

$$\begin{vmatrix} Y_{11} & Y_{12} & Y_{13} \\ Y_{21} & Y_{22} & Y_{23} \\ Y_{31} & Y_{32} & Y_{33} \end{vmatrix} \begin{vmatrix} V_1 \\ V_2 \\ V_3 \end{vmatrix} = \begin{vmatrix} I_1 \\ I_2 \\ I_3 \end{vmatrix} \tag{2.6}$$

where $Y_{ij}$ is the elements of the bus admittance matrix, $V_i$ is the bus voltages, $I_i$ is the currents injected at each node. The node equation at bus i can be written as

$$I_i = \sum_{j=1}^{n} (Y_{ij} V_j) \tag{2.7}$$

Power-flow Analysis Equations show the relationship between per-unit real and reactive power supplied to the system at bus i and the per-unit current injected into the system at that bus

$$S_i = V_i I_i^* = P_i + jQ_i \tag{2.8}$$

where $V_i$ is the per-unit voltage at the bus, $I_i^*$ is a complex conjugate of the per-unit current injected at the bus, $P_i$ and $Q_i$ are per-unit real and reactive powers.

Therefore,

$$I_i^* = (P_i + jQ_i)/V_i \rightarrow I_i = (P_i - jQ_i)/V_i^* \quad (2.9)$$

$$\rightarrow P_i - jQ_i = \sum_{j=1}^{n} V_i^* (Y_{ij} V_j) \quad (2.10)$$

$$\text{Let } Y_{ij} = |Y_{ij}| \angle \theta_{ij} \text{ and } V_i = |V_i| \angle \delta_i \quad (2.11)$$

$$\text{Then } P_i - jQ_i = \sum_{j=1}^{n} |(Y_{ij} \| V_j \| V_i)| \angle (\theta_{ij} + \delta_j - \delta_i) \quad (2.12)$$

$$\text{Hence} \quad P_i = \sum_{j=1}^{n} |(Y_{ij} \| V_j \| V_i)| \cos (\theta_{ij} + \delta_j - \delta_i) \quad (2.13)$$

$$\text{And} \quad Q_i = -\sum_{j=1}^{n} |(Y_{ij} \| V_j \| V_i)| \sin (\theta_{ij} + \delta_j - \delta_i) \quad (2.14)$$

In load flow analysis, real power P, reactive power Q, and bus voltage magnitude and angles are calculated for different types of buses by solving these equations for all buses in the network.

# CHAPTER 3

# GRID CONNECTED

An analysis for grid-connected microgrid for different load scenarios is presented in this chapter. Both load changes at different buses and increasing penetration of solar generator values at bus 6 are studied for the IEEE 9-bus system, with the goal of highlighting the impact of changes for solar generators and shedding some light on the values of bus voltages for stability analysis. In addition, several contingency analysis scenarios are also considered.

## 3.1 All Facility Included (AFI) Scenario

In the first place, a general analysis of the voltage and angle performance of the IEEE 9-bus system under two cases will be presented. This performance has been compared with peak load setup and minimum load (30% of peak load) case simultaneously. The same simulation has been conducted using all the parameters for synchronous machines and solar generators. In order to quantify how the inclusion of solar generators affects voltage and angle profiles, different operating modes for solar have been used.

The IEEE 9-bus test case power system was used as the case study to show the developed methodology. The original 9-bus system, from now on referred to as the original case, contains three synchronous machines as sources of electric power. The effect of solar penetration in this system has been studied by connecting some solar generators to it, while the total amount of synchronous machine values in the system has been kept constant. Thus, when including a certain amount of solar power, the amount of power generated by synchronous generators has been adjusted by the swing bus when the system is grid connected. The slack bus or swing bus is a bus

with a large generator that can freely adjust its real and reactive power output to enable the power flow to solve. At the slack bus, the voltage will always remain at 1 P.U. with a phase angle of 0. The real and reactive power will then swing to accommodate line losses and other issues and cause the power flow solution to converge. If there are issues in the system, it is possible for the slack bus to exceed its limits while performing power flow analysis.

### 3.1.1 AFI Peak Load Case

For this case study, two kinds of load scenarios have been considered with the same setup for all other components due to several factors discussed in the previous chapter. The SKM solar generator models used for the simulations, which are discussed in Chapter 2, are adequate to represent the increased penetration of solar in the system. So, they were used as such in all the simulations in this thesis. The model network has been built in SKM that includes the given transformer, branch, bus, and synchronous generator data for the original test case system.

For the peak load cases, all three synchronous generators are supplying full rated values mentioned in Table 3.1. Also, three loads are connected respectively at bus 5, bus 6, and bus 8. The solar penetration has been done on bus 6. The rated values for generators, loads, and buses are detailed in Table 3.1. Simulation for this setup has been done, and the voltage, power loss throughout the system, and angle changes at bus 6 have been observed as the solar generation level keeps changing. The analysis has been done on bus 6 as the solar generator is added here.

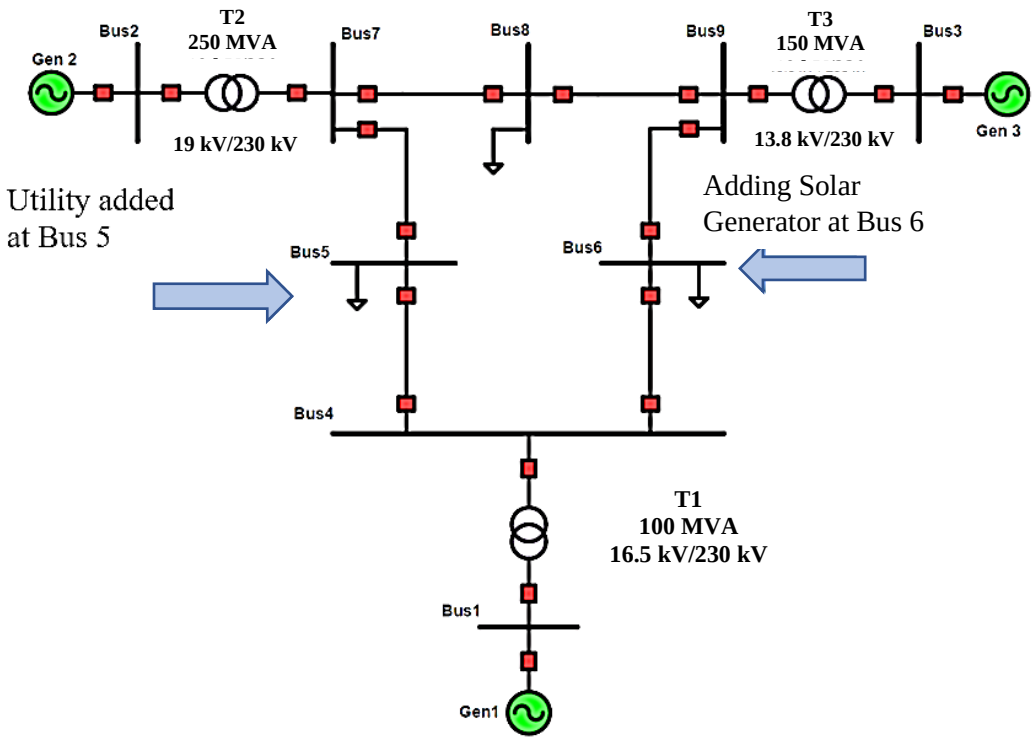


Figure 3.1 Network for AFI simulation [31]

Table 3.1 Input data used for AFI peak load

| Bus no | Bus Code | Voltage (pu) | Generation | | | Load | |
|---|---|---|---|---|---|---|---|
| | | | MW | MVAR | | MW | MVAR |
| | | | | Min | Max | | |
| 1 | PV | 1.04 | 10 | -5 | 5 | 0 | 0 |
| 2 | PV | 1.025 | 163 | -67 | 67 | 0 | 0 |
| 3 | PV | 1.025 | 85 | -40 | 40 | 0 | 0 |
| 4 | PQ | 1 | 0 | 0 | 0 | 0 | 0 |
| 5 | PQ | 1 | 0 | 0 | 0 | 125 | 0 |
| 6 | PQ | 1 | 0 | 0 | 0 | 90 | 0 |
| 7 | PQ | 1 | 0 | 0 | 0 | 0 | 0 |
| 8 | PQ | 1 | 0 | 0 | 0 | 100 | 0 |
| 9 | PQ | 1 | 0 | 0 | 0 | 0 | 0 |

As described in section 3.1.1, the synchronous generators are connected with their highest rated values such as 163 MW, 85 MW, and 10 MW respectively. The reactive power range values have also been set in Table 3.1. Three loads are connected in Bus 5, 6, and 8 with values of 125 MW, 90 MW, and 100 MW respectively. Now, while adding the solar generator at bus 6, the operating mode of the solar generator has been changed to get the desired voltage range at bus 6. It has been observed that when the solar generator is working as a leading power factor of solar generator as 0.9, the voltages at bus 6 as well as all other bus voltages lie within the accepted range (0.95-1.05 pu) for the base case (no solar).

Table 3.2 Output data for AFI peak load (leading)

| Solar Generator at BUS 6 | Operating Mode of solar generator | Voltage at BUS 6 | Angle | Slack BUS | | Loss | |
|---|---|---|---|---|---|---|---|
| | | | | MW | MVAR | MW | MVAR |
| 0 | N/A | 1.05 | -3.20 | 61 | -17 | 4 | 122 |
| 50 | Lead | 1.03 | 1.63 | 11 | -73 | 4 | 120 |
| 100 | Lead | 1.01 | 6.53 | -37 | 13 | 6 | 101 |
| 200 | Lead | 0.89 | 18.29 | -128 | 84 | 14 | 70 |
| 350 | Lead | 0.80 | 38.33 | -253 | 175 | 39 | 161 |
| 400 | Does not converge | | | | | | |

Table 3.3 Output data for AFI peak load (lagging)

| Solar Generator at BUS 6 | Operating Mode of solar generator | Voltage at BUS 6 | Angle | Slack BUS | | Loss | |
|---|---|---|---|---|---|---|---|
| | | | | MW | MVAR | MW | MVAR |
| 0 | N/A | 1.05 | -3.20 | 61 | -17 | 3 | 122 |
| 50 | Lag | 1.10 | 1.00 | 11 | -43 | 4 | 130 |
| 100 | Lag | 1.11 | 5.28 | -37 | -38 | 5 | 110 |
| 200 | Lag | 1.32 | 10.20 | -130 | -162 | 11 | 124 |
| 350 | Lag | 1.28 | 22.2 | -270 | -85 | 22 | 118 |
| 600 | Lead/lag | Does not converge | | | | | |

The Power Factor can be lagging, leading, or unity. When the current generated by the solar generator lags behind the bus voltage, the power factor of the circuit is called lagging. From Table 3.2, it can be said that the peak configuration of AFI connected grid system here can be handled with solar penetration below 200 MW. For the base case with no solar installed, the bus 6 voltage is 1.05 pu, which is the maximum allowable voltage value in the range. That is why it has been chosen as a base case for both leading and lagging cases. The solar generator here must be kept as a leading operating mode. Changing the power factor from 0.9 to 0.8 does not impact the system values significantly. Also, the angles increase with increasing penetration of solar because more reactive power is being added to the system. As there is more flow of reactive power, the system angle is also increasing with more penetration of solar. All loads are currently operating in unity mode here. For the values of slack bus real and reactive power, the relation can be described as a sink (slack) and source (solar). Adding solar will result in more flow in the slack bus, and it can be seen from the values from Table 3.2 and 3.3.

From Table 3.3, the voltage values are not in range when lagging operating mode for the solar generator has been used. For all cases discussed here, MVAR losses are higher than MW losses due to the line impedance values. As given the line values in Chapter 2, reactance values are higher than the resistance values. In that case, real power can travel a long way through the transmission line, but reactive power case is not applicable for this as resistance values are really small. So, MVAR losses>>MW losses due to X>>R. For the AFI peak load case, no additional reactor has been used so voltage values with higher solar penetrations are out of range for few cases shown in Table 3.3. The power voltage curve with increasing penetration of solar is shown in Figure 3.2.

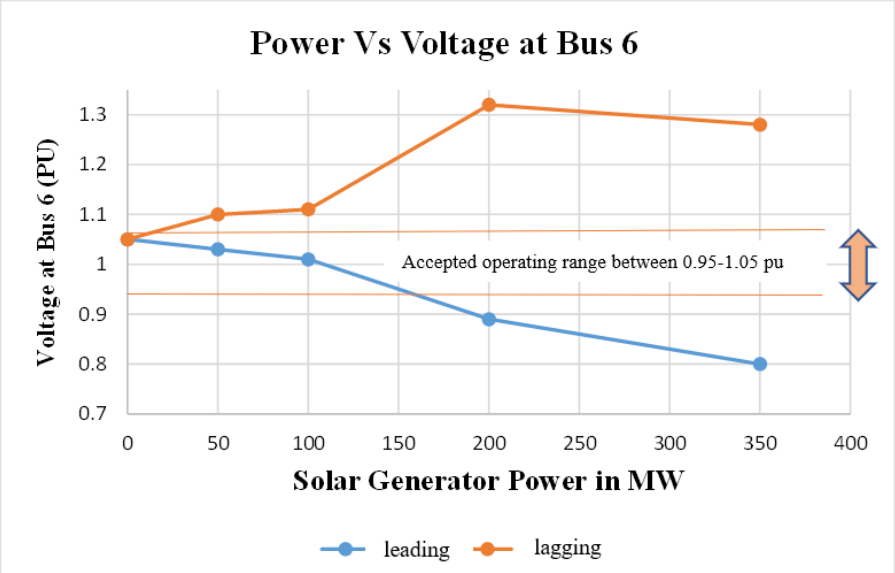


Figure 3.2 Power Voltage curve for AFI peak load

Also, load flow analysis is not a linear function, so the values here between different ranges of solar penetration can be considered as approximate values, not exact. Because if the values have been considered as exact values, then it might seem that the voltage vs power value is following a linear pattern, which is not correct in the load flow case. So, under the configuration described in

Table 3.1, the bus 6 voltage has its highest value of 1.05 pu. When bus 6 voltage values are considered for leading power factor, solar generator up to 150 MW has an acceptable voltage range. But when the solar generator operates in lagging factor, the voltages are out of range, so the leading operating mode is accepted in this configuration with AFI peak load case.

### 3.1.2 AFI Min Load Case

This scenario has been considered for the minimum (30% of peak load) load cases when all three synchronous generators are supplying full rated value mentioned in Table 3.4. Also, three loads are connected respectively at bus 5, bus 6, and bus 8. The rated values for generators, loads, and buses for AFI min load case are listed in Table 3.4.

Table 3.4 Input data used for AFI min load

| Bus no | Bus Code | Voltage (pu) | Generation | | | Load | |
|---|---|---|---|---|---|---|---|
| | | | MW | MVAR | | MW | MVAR |
| | | | | Min | Max | | |
| 1 | PV | 1.04 | 10 | -5 | 5 | 0 | 0 |
| 2 | PV | 1.025 | 163 | -67 | 67 | 0 | 0 |
| 3 | PV | 1.025 | 85 | -40 | 40 | 0 | 0 |
| 4 | PQ | 1 | 0 | 0 | 0 | 0 | 0 |
| 5 | PQ | 1 | 0 | 0 | 0 | ~~125~~ 37 | 0 |
| 6 | PQ | 1 | 0 | 0 | 0 | ~~90~~ 27 | 0 |
| 7 | PQ | 1 | 0 | 0 | 0 | 0 | 0 |
| 8 | PQ | 1 | 0 | 0 | 0 | ~~100~~ 30 | 0 |
| 9 | PQ | 1 | 0 | 0 | 0 | 0 | 0 |

Simulation has been conducted for this setup, and the voltage, power loss, and angle changes at bus 6 have been observed as the solar generation level changes. The results for each case have been listed in respective tables. The analysis has been done on bus 6 as the solar generator is added there.

Three loads are connected to Bus 5, 6, and 8 with values of 37 MW, 27 MW, and 30 MW respectively. While adding the solar generator at bus 6, the operating mode of the solar generator has been changed to achieve the desired voltage range at bus 6. It has been observed that when the solar generator is working as a leading mode with a power factor of 0.9, the voltages at bus 6, as well as all other bus voltages, lie within the accepted range (0.95-1.05 pu) for the base case (no solar). To fix the base case (no solar) voltage ranges, a reactor has been added to the system. The reactor value has been set using the equation for

$$XL = (|kV|^2)/ MVAR \tag{3.1}$$

$$L = XL/ (2\pi F) \tag{3.2}$$

When the system is operating with the same setup but without any reactor (inductor in this case), all bus voltages are not within range. Among them, bus 9 voltage value is 1.14 pu, which is unstable and not acceptable. To fix this issue, a reactor (inductor) with a value of 1.5 H has been added to bus 9. The reason for choosing bus 9 is that bus 9 has the highest out-of-range voltage value without a reactor. The values for voltage, angle, and power losses with the reactor have been listed in Table 3.5. The equation for calculating inductor value has been shown in equation 3.1. The generators of the system can go to both modes, depending on the requirement of the system. For system voltage, the generator will try to hold the voltage at the Point of Interconnection (POI), so if voltage goes up and down at POI, the solar generator is responsible for the voltage value. So,

the solar generator might have a lagging mode, and that's why the inductor can be used in this case. As seen in table 3.5(a), a 400 MW solar generator with leading mode does not converge, so it is not recommended to add more than 350 MW leading solar generator with this setup. Adding a reactor here does not have an impact on the no-convergence case. That means this system will not have stable parameters with more than 350 MW solar penetration regardless of using a reactor or not.

Table 3.5(a) Output data for AFI min load (fixed Q)

| Solar Generator at BUS 6 | Operating Mode of solar generator | PF | Reactor added at Bus 9 | Voltage at BUS 6 | Angle | Slack BUS | | Loss | |
|---|---|---|---|---|---|---|---|---|---|
| | | | | | | MW | MVAR | MW | MVAR |
| 0 | N/A | 0 | 1.5 H | 1.04 | 8.26 | -154 | 15 | 9 | 97 |
| 100 | Lead | 0.9 | | 0.99 | 18.61 | -249 | 57 | 14 | 83 |
| | Lag | 0.9 | | 1.09 | 16.69 | -249 | 17 | 14 | 90 |
| 200 | Lead | 0.97 | | 0.97 | 29.09 | -340 | 94 | 23 | 133 |
| | Lag | 0.97 | | 1.08 | 26.06 | -341 | 49 | 22 | 122 |
| 400 | Lead/unity | | | Does not converge | | | | | |
| | Lag | 0.99 | | 1.01 | 49.01 | -509 | 156 | 55 | 301 |
| 600 | Lead/lag | | | Does not converge | | | | | |

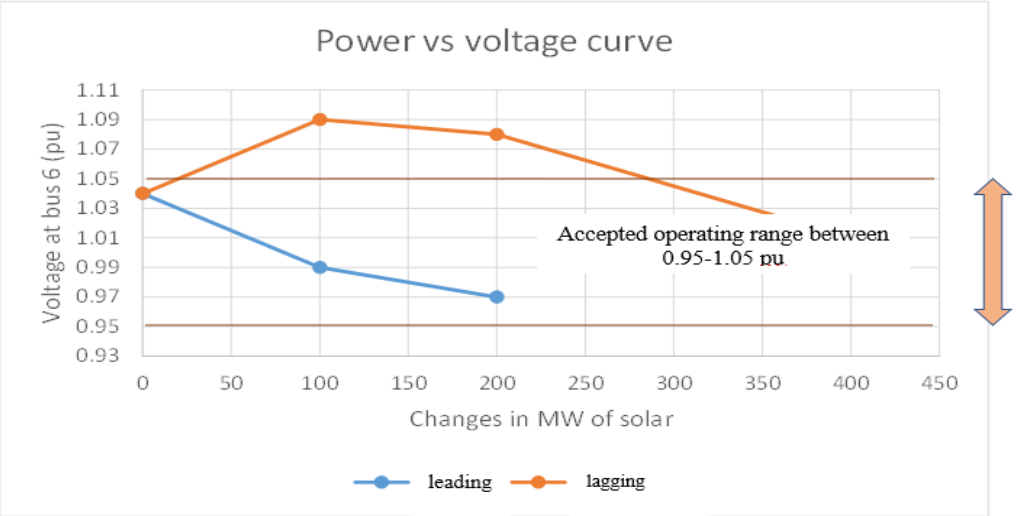


Figure 3.3 (a) Power Voltage curve for AFI min load (fixed Q)

From Figure 3.3 (a), the lagging curve is going up and then the value drops because the power factor is changing at every point with increasing solar penetration. The reason for dropping the voltage at a certain point is power factor changes at every point, as shown in Table 3.5 (a). Figure 3.3 (a) shows the same behavior for other cases for the rest of the studies. Table 3.5 (b) shows the values for all parameters when the power factor is fixed, but reactive power changes with solar penetration level. The fixed power factor case reveals that most of the solar penetration level will be out of the voltage acceptance range. So, it can be said from Table 3.5 (b) that changing power factor can bring operation in range. The power voltage curve for a fixed power factor is shown in Figure 3.3(b).

Table 3.5(b) Output data for fixed power factor 0.9

| Solar Generator at BUS 6 | Operating Mode of solar generator | Q value in MVAR | Reactor added at Bus 9 | Voltage at BUS 6 | Angle | Slack BUS | | Loss | |
|---|---|---|---|---|---|---|---|---|---|
| | | | | | | MW | MVAR | MW | MVAR |
| 0 | N/A | x | 1.5 H | 1.04 | 8.26 | -154 | 15 | 9 | 97 |
| 100 | Lead | -48 | | 0.99 | 18.60 | -249 | 57 | 14 | 83 |
| | Lag | 48 | | 1.09 | 16.70 | -249 | 18 | 14 | 89 |
| 200 | Lead | -96 | | 0.88 | 31.66 | -336 | 130 | 23 | 101 |
| | Lag | 96 | | 1.12 | 24.94 | -341 | 30 | 22 | 116 |
| 400 | Lead/unity | | | Does not converge | | | | | |
| | Lag | 192 | | 1.16 | 42.32 | -513 | 85 | 50 | 266 |
| 600 | Lead/lag | | | Does not converge | | | | | |

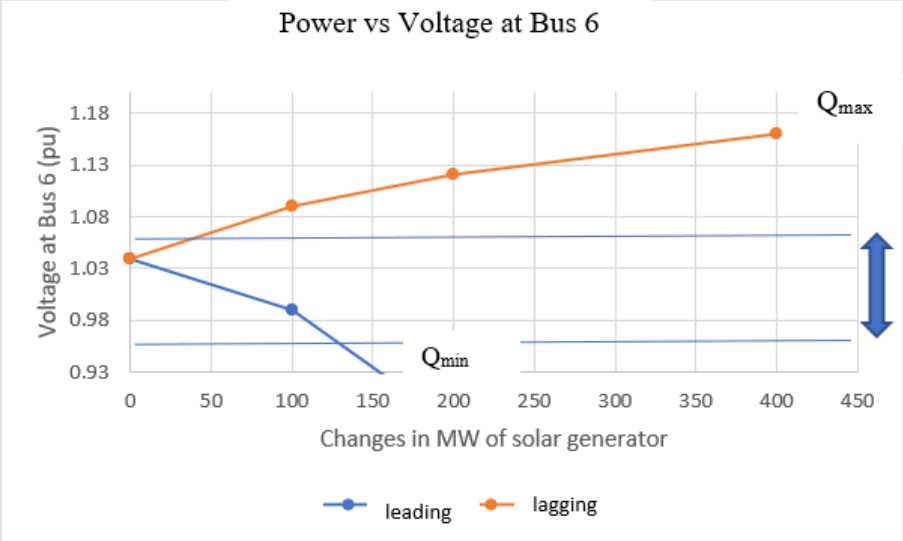


Figure 3.3 (b) Power Voltage curve for AFI min load (fixed Power factor 0.9)

Changing the starting power factor value from 0.9 to 0.7 can limit the solar penetration level from 400 MW to 200 MW. The results with 0.7 power factor are listed in Table 3.6.

Table 3.6 Output data for AFI min load (fixed Q and starting power factor is 0.7)

| Solar Generator at BUS 6 | Operating Mode of solar generator | Reactor added at Bus 9 | Voltage at BUS 6 | Angle | Slack BUS | | Loss | |
|---|---|---|---|---|---|---|---|---|
| | | | | | MW | MVAR | MW | MVAR |
| 0 | N/A | 1.5 H | 1.04 | 8.42 | -157 | 15 | 9 | 96 |
| 100 | Lead | | 1.02 | 20.50 | -250 | 94 | 16 | 80 |
| | Lag | | 1.07 | 15.98 | -251 | 0.7 | 15 | 86 |
| 200 | Lead | | 1.01 | 32.23 | -338 | 137 | 28 | 144 |
| | Lag | | 1.06 | 24.9 | -343 | 29 | 23 | 117 |
| 400 | Lead/unity | | Does not converge | | | | | |
| | Lag | | | | | | | |
| 600 | Lead/lag | | Does not converge | | | | | |

From Table 3.6, it can be said that for the min. configuration of AFI case, the voltage would be in the range for solar penetration below 400 MW if operating power factor is 0.7. The solar generator here must be checked for operating mode. Changing the power factor from 0.9 to 0.8 does not impact the system values significantly. Also, the angles increase with increasing penetration of solar because more reactive power is being added to the system. As there is more flow of reactive power, the system angle is also increasing with more penetration of solar. In this scenario, all loads are operating at unity power factor.

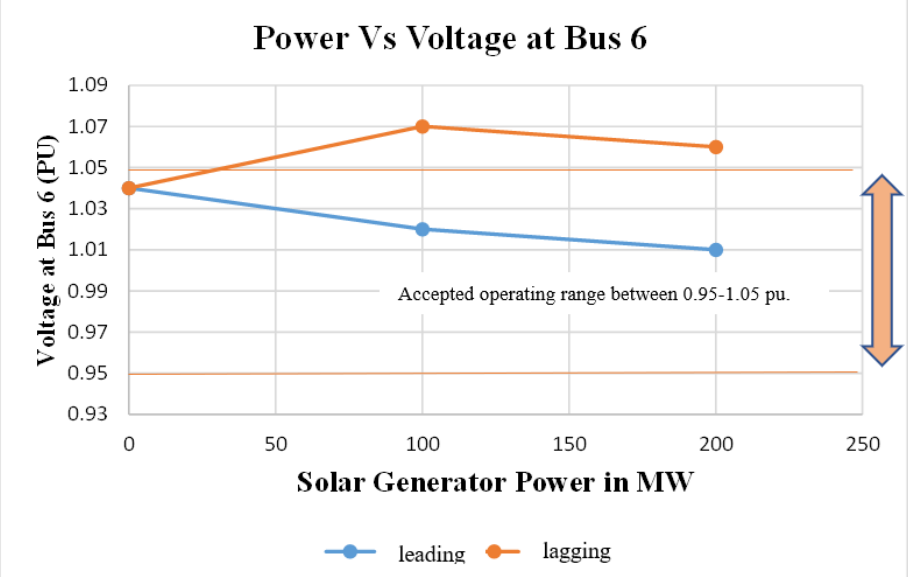


Figure 3.4 Power Voltage curve for AFI min load (fixed Q)

## 3.2 Generator 3 Out Scenario

### 3.2.1 Contingency Analysis (N-1 Gen 3 out- Peak Load)

For this case study, two kinds of load scenarios have been considered with the same setup for all other components due to several factors discussed in the previous chapter. For the peak load cases when only two synchronous generators are supplying full rated value mentioned in Table 3.7. Generator 3 is taken out of service for contingency analysis. Also, three loads are connected respectively at bus 5, bus 6, and bus 8. The rated values for all components and parameters are given in Table 3.7. Simulation for this setup has been done, and the voltage, power loss, and angle changes at bus 6 have been observed as the solar generation level keeps changing. The analysis has been done on bus 6 as the solar generator is added here.

Table 3.7 Input data used for Gen 3 out peak load

| Bus no | Bus Code | Voltage (pu) | Generation | | | Load | |
|---|---|---|---|---|---|---|---|
| | | | MW | MVAR | | MW | MVAR |
| | | | | Min | Max | | |
| 1 | PV | 1.04 | 10 | -5 | 5 | 0 | 0 |
| 2 | PV | 1.025 | 163 | -67 | 67 | 0 | 0 |
| 3 | PV | 1.025 | ~~85~~ 0 | ~~-40~~ 0 | ~~40~~ 0 | 0 | 0 |
| 4 | PQ | 1 | 0 | 0 | 0 | 0 | 0 |
| 5 | PQ | 1 | 0 | 0 | 0 | 125 | 0 |
| 6 | PQ | 1 | 0 | 0 | 0 | 90 | 0 |
| 7 | PQ | 1 | 0 | 0 | 0 | 0 | 0 |
| 8 | PQ | 1 | 0 | 0 | 0 | 100 | 0 |
| 9 | PQ | 1 | 0 | 0 | 0 | 0 | 0 |

Table 3.8 shows the similar simulation for power factor 0.9. The comparison of operations for different power factor helps to bring bus voltages in range. This can be seen after comparing Table 3.8 and Table 3.9.

Table 3.8 Output data for fixed Q (starting pf 0.9)

| Solar Generator at BUS 6 | Reactor added at Bus 9 | Operating Mode of solar generator | Voltage at BUS 6 | Angle | Slack BUS | | Loss | |
|---|---|---|---|---|---|---|---|---|
| | | | | | MW | MVAR | MW | MVAR |
| 0 | 1 H | N/A | 0.99 | -9.30 | 148 | -10 | 5 | 101 |
| 50 | | lead | 0.99 | 35.19 | -272 | 102 | 33 | 133 |
| | | lag | 1.03 | -4.54 | 97 | -15 | 4 | 113 |
| 200 | | lead | 0.99 | 10.31 | -49 | 24 | 7 | 90 |
| | | lag | 1.04 | 9.35 | -49 | 46 | 6 | 99 |
| 450 | | unity | 1.00 | 34.65 | -274 | 97 | 31 | 145 |
| | | lag | 0.99 | 35.19 | -272 | 102 | 33 | 133 |
| 600 | | Lead/lag | | Does not converge | | | | |

From Table 3.8, it can be said that peak configuration of generator 3 out contingency case can be handled with solar penetration up to 450 MW. For the base case with no solar generation installed, the bus 6 voltage is 0.99 pu, which is within the allowable voltage range. That is why it has been chosen as the base case for both the leading and lagging cases. The solar generator operating mode can be changed to leading or lagging as shown in respective tables. The power voltage curve is shown in Figure 3.5.

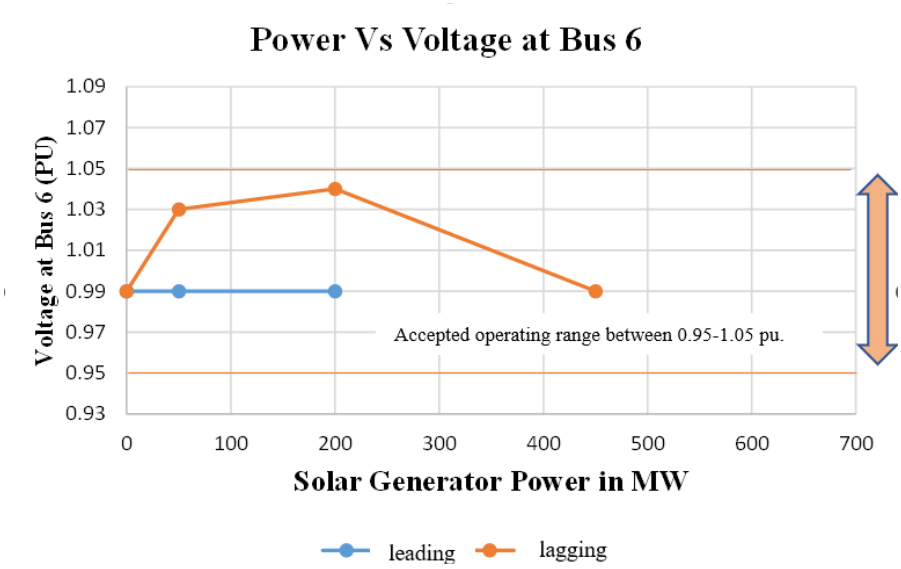


Figure 3.5 Power Voltage curve for Gen 3 out- Peak Load (power factor 0.9)

From Figure 3.5, all the voltages for leading and lagging power factors lie within the allowable range of 0.95-1.05 pu. So, it can be considered the best case for load flow purposes. Bus voltages have a better range for solar in load flow cases. It can be assigned as the host capacity of the network system. Though the synchronous generator has been removed, additional solar can be integrated with an acceptable output bus voltage range because the system has a large enough capacity.

Table 3.9 Output data for fixed Q (starting pf 0.8)

| Solar Generator at BUS 6 | Reactor added at Bus 9 | Operating Mode of solar generator | Voltage at BUS 6 | Angle | Slack BUS | | Loss | |
|---|---|---|---|---|---|---|---|---|
| | | | | | MW | MVAR | MW | MVAR |
| 0 | 1.5 H | N/A | 1.01 | -9.17 | 147 | -15 | 4 | 112 |
| 50 | | lead | 0.98 | -1.09 | 96 | -661 | 3 | 115 |
| | | lag | 1.07 | -4.62 | 97 | -33 | 3 | 125 |
| 200 | | lead | 0.97 | -7.64 | 127 | -1 | 3 | 110 |
| | | lag | 1.06 | -7.38 | 127 | -34 | 3 | 121 |
| 450 | | lead | 0.72 | 52.32 | -249 | 275 | 55 | 265 |
| | | lag | 1.04 | 33 | -275 | 78 | 30 | 138 |
| 600 | | Lead/lag/ unity | Does not converge | | | | | |

Changing the power factor from 0.9 to 0.8 changes the penetration level significantly. All loads are operating in unity pf mode here. From Table 3.9, the voltage values are not in range for some solar generators operating on lagging or leading. For all cases discussed here, MVAR losses are higher than MW losses due to the line impedance values. As given the line values in Chapter 2, reactance values are higher than the resistance values. With a power factor value of 0.8, the solar penetration level can be accepted up to 200 MW, whereas if the power factor is 0.9, it will be up to 400 MW. The power voltage curve with increasing solar penetration is shown in Figure 3.6.

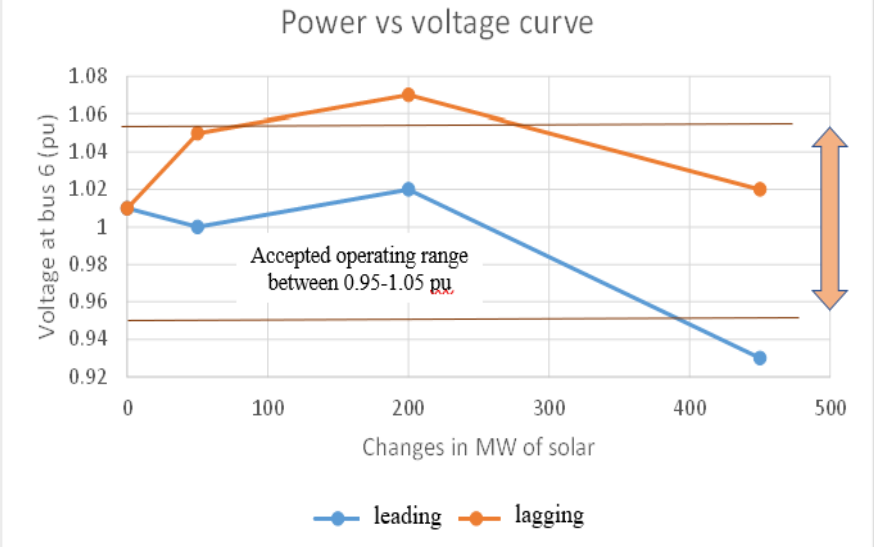


Figure 3.6 Power Voltage curve for Gen 3 out- Peak Load (power factor 0.8)

### 3.2.2 Contingency Analysis (N-1 Gen 3 out- Min Load)

This scenario has been considered for the min (30% of peak load) load cases when two synchronous generators are supplying the full rated value mentioned in Table 3.10. The solar penetration has been done on bus 6 just the same as the previous cases. The rated values for generators, loads and buses are detailed in Table 3.10. Simulation for this setup has been done, and the voltage, power loss, angle changes at bus 6 has been observed as the solar generation level keeps changing. The analysis has been done on bus 6 as the solar generator is added here.

Three loads are connected in Bus 5, 6, and 8 with values of 37 MW, 27 MW and 30 MW, respectively. While adding the solar generator at bus 6, the operating mode of the solar generator has been changed to get the desired voltage range at bus 6. It has been observed that when the solar generator is working as leading mode with a power factor of 0.9, the voltages at bus 6, as well as all other bus voltage lies within the accepted range (0.95-1.05 pu) for the base case (no solar).

Table 3.10 Input data used for Gen 3 out Min load

| Bus no | Bus Code | Voltage (pu) | Generation | | | Load | |
|---|---|---|---|---|---|---|---|
| | | | MW | MVAR | | MW | MVAR |
| | | | | Min | Max | | |
| 1 | PV | 1.04 | 10 | -5 | 5 | 0 | 0 |
| 2 | PV | 1.025 | 163 | -67 | 67 | 0 | 0 |
| 3 | PV | 1.025 | ~~85~~ 0 | ~~-40~~ 0 | ~~40~~ 0 | 0 | 0 |
| 4 | PQ | 1 | 0 | 0 | 0 | 0 | 0 |
| 5 | PQ | 1 | 0 | 0 | 0 | ~~125~~ 37 | 0 |
| 6 | PQ | 1 | 0 | 0 | 0 | ~~90~~ 27 | 0 |
| 7 | PQ | 1 | 0 | 0 | 0 | 0 | 0 |
| 8 | PQ | 1 | 0 | 0 | 0 | ~~100~~ 30 | 0 |
| 9 | PQ | 1 | 0 | 0 | 0 | 0 | 0 |

From Table 3.11, it can be said that min configuration of generator 3 out contingency case here can be handled with solar penetration up to 400 MW. For the base case with no solar installed, the bus 6 voltage is 1.04 pu which is within the allowable voltage range. That is why it has been chosen as the base case for both leading and lagging cases. The solar generator operating mode can be changed here. The power voltage curve is shown in Figure 3.7

Table 3.11 Output data for fixed Q (starting pf 0.9)

| Solar Generator at BUS 6 | Reactor added at Bus 9 | Operating Mode of solar generator | Voltage at BUS 6 | Angle | Slack BUS | | Loss | |
|---|---|---|---|---|---|---|---|---|
| | | | | | MW | MVAR | MW | MVAR |
| 0 | 2 H | N/A | 1.04 | 2.55 | -74 | -2 | 4 | 119 |
| 50 | | lead | 1.03 | 7.32 | -123 | 10 | 5 | 113 |
| | | lag | 1.06 | 6.94 | -123 | -3 | 5 | 103 |
| 200 | | lead | 1.04 | 21.27 | -265 | 40 | 13 | 65 |
| | | lag | 1.06 | 20.72 | -265 | 33 | 13 | 65 |
| 400 | | lead | 0.93 | 45.97 | -433 | 156 | 44 | 217 |
| | | lag | 0.99 | 43.01 | -437 | 132 | 41 | 208 |
| 450 | | Lead/lag | Does not converge | | | | | |

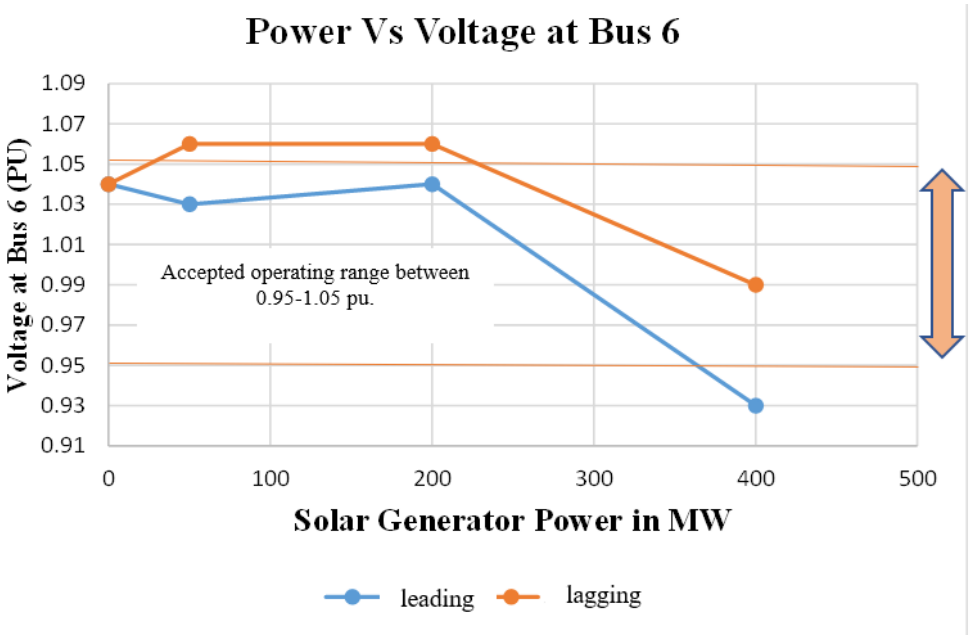


Figure 3.7 Power Voltage curve for Gen 3 out- Min Load

Changing power factor from 0.9 to 0.7 changes the penetration level significantly. All loads are operating in unity mode here. From Table 3.12, the voltage values are not in range after 50 MW regardless of solar generator is operating under lagging or leading power factor. For all cases discussed here, MVAR losses are higher than MW losses due to the line impedance values. With power factor value of 0.9, solar penetration level can be accepted up to 400 MW whereas if the power factor is 0.7, it will be up to 50 MW. So, this configuration setting can be considered as worst-case scenario. The power voltage curve with increasing penetration of solar is shown in Figure 3.8.

Table 3.12 Output data for fixed Q (starting pf 0.7)

| Solar Generator at BUS 6 | Reactor added at Bus 9 | Operating Mode of solar generator | Voltage at BUS 6 | Angle | Slack BUS | | Loss | |
|---|---|---|---|---|---|---|---|---|
| | | | | | MW | MVAR | MW | MVAR |
| 0 | 2 H | N/A | 1.04 | 2.71 | -77 | -1 | 4 | 107 |
| 50 | | lead | 1.02 | 7.67 | -126 | 17 | 5 | 111 |
| | | lag | 1.08 | 6.93 | -126 | -8 | 5.5 | 116 |
| 200 | | lead | 1.08 | 6.93 | -126 | -8 | 6 | 116 |
| | | lag | 1.08 | 20.55 | -268 | 27 | 13 | 82 |
| 400 | | unity | 0.96 | 44.42 | -438 | 145 | 43 | 228 |
| | | | Lead/lag does not converge | | | | | |

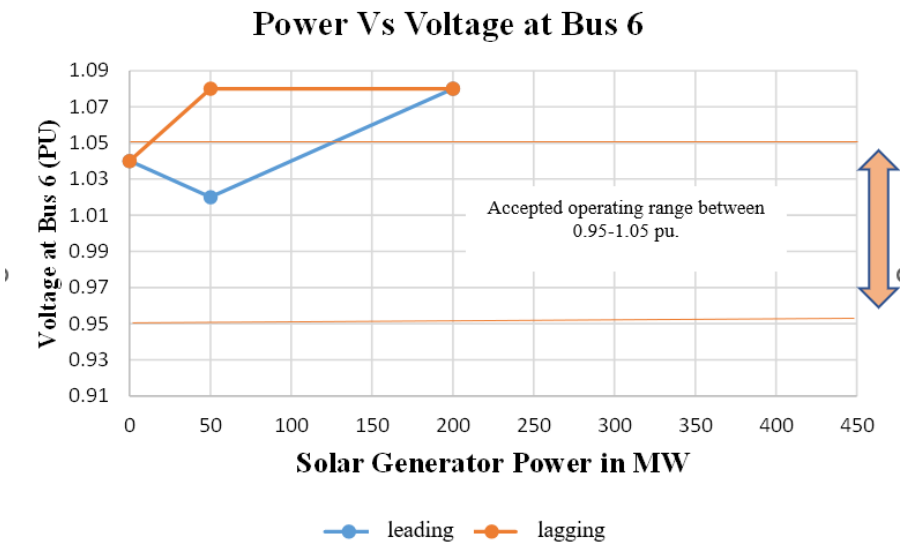


Figure 3.8 Power Voltage curve for Gen 3 out- Min Load

### 3.3 Generator 2 Out Scenario

Generator 2 out scenario has been considered for peak load and minimum load as described in the following sections.

#### 3.3.1 Contingency Analysis (N-1 Gen 2 out- Peak Load)

For this case study, two kinds of load scenarios have been considered with the same setup for all other components, due to several factors discussed in the previous chapter. Generator 2 is taken out of service for contingency analysis. Also, three loads are connected respectively at bus 5, bus 6 and bus 8. The solar penetration has been done on bus 6. The rated values for generators, loads and buses are detailed in Table 3.13. Simulation for this set up has been done and the voltage, power loss, angle changes at bus 6 has been observed as the solar generation level keeps changing. The analysis has been done on bus 6 as the solar generator is added here.

Table 3.13 Input data used for Gen 2 out peak load

| Bus no | Bus Code | Voltage (pu) | Generation | | | Load | |
|---|---|---|---|---|---|---|---|
| | | | MW | MVAR | | MW | MVAR |
| | | | | Min | Max | | |
| 1 | PV | 1.04 | 10 | -5 | 5 | 0 | 0 |
| 2 | PV | 1.025 | ~~163~~ 0 | ~~-67~~ 0 | ~~67~~ 0 | 0 | 0 |
| 3 | PV | 1.025 | 85 | -40 | 40 | 0 | 0 |
| 4 | PQ | 1 | 0 | 0 | 0 | 0 | 0 |
| 5 | PQ | 1 | 0 | 0 | 0 | 125 | 0 |
| 6 | PQ | 1 | 0 | 0 | 0 | 90 | 0 |
| 7 | PQ | 1 | 0 | 0 | 0 | 0 | 0 |
| 8 | PQ | 1 | 0 | 0 | 0 | 100 | 0 |
| 9 | PQ | 1 | 0 | 0 | 0 | 0 | 0 |

Table 3.14 Output data for fixed Q (starting pf 0.9-reactor 3.5 H)

| Solar Generator at BUS 6 | Reactor added at Bus 9 | Operating Mode of solar generator | Voltage at BUS 6 | Angle | Slack BUS | | Loss | |
|---|---|---|---|---|---|---|---|---|
| | | | | | MW | MVAR | MW | MVAR |
| 0 | 3.5 H | N/A | 1.05 | -10.37 | 224 | -96 | 2 | 116 |
| 50 | | lead | 1.05 | -5.67 | 173 | -51 | 1 | 122 |
| | | lag | 1.07 | -5.84 | 173 | -61 | 0.8 | 89 |
| 350 | | lead | 1.05 | 21.5 | -113 | 15 | 14 | 93 |
| | | lag | 1.08 | 20.83 | -113 | 3 | 14 | 92 |
| 400 | | lead | 1.05 | 26.17 | -157 | 30 | 19 | 116 |
| | | lag | 1.07 | 25.64 | -158 | 24 | 19 | 115 |
| 600 | | Lead/lag | Does not converge | | | | | |

From Table 3.14, it can be said that peak configuration of generator 2 out contingency case here can be handled with solar penetration up to 400 MW. For the base case with no solar installed, the bus 6 voltage is 1.05 pu which is the maximum allowable voltage range. That is why it has been chosen as the base case for both leading and lagging cases. The solar generator operating mode can be changed here. The power voltage curve is shown in figure 3.9.

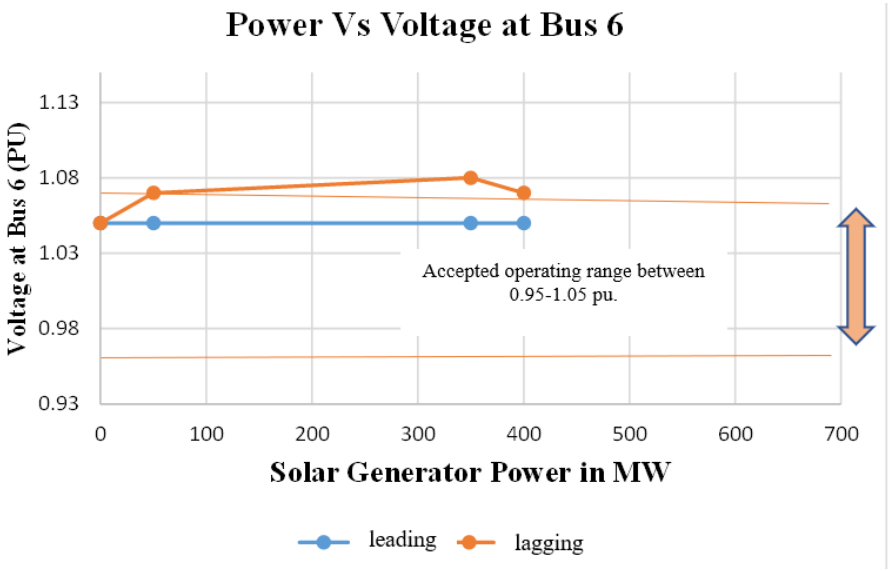


Figure 3.9 Power Voltage curve for Gen 2 out- Peak Load (3.5 H)

As the leading solar generator does not have effect on the bus 6 voltage value, reactor values have been changed to fix this.

Table 3.15 Output data for fixed Q (starting pf 0.9- reactor 5 H)

| Solar Generator at BUS 6 | Reactor added at Bus 9 | Operating Mode of solar generator | Voltage at BUS 6 | Angle | Slack BUS | | Loss | |
|---|---|---|---|---|---|---|---|---|
| | | | | | MW | MVAR | MW | MVAR |
| 0 | 5 H | N/A | 1.05 | -10.33 | 222 | -57 | 3 | 131 |
| 50 | | lead | 1.03 | -5.56 | 171 | -46 | 1 | 137 |
| | | lag | 1.11 | -5.97 | 171 | -95 | 2 | 148 |
| 350 | | lead | 1.04 | 21.68 | -115 | 15 | 15 | 108 |
| | | lag | 1.09 | 20.48 | -115 | -5 | 14 | 106 |
| 400 | | lead | 1.04 | 26.58 | -159 | 36 | 20 | 130 |
| | | lag | 1.08 | 25.35 | -160 | 19 | 20 | 126 |
| 600 | | Lead/lag | Does not converge | | | | | |

Bus 6 voltage value lies within the voltage range after changing the reactor value from 3.5 H to 5 H. The power voltage curve with 5 H value is shown in Figure 3.10.

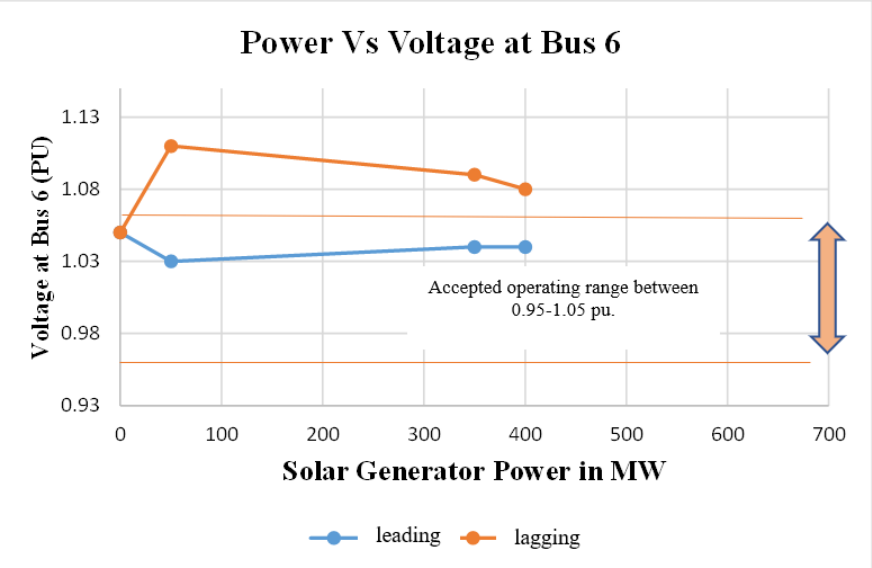


Figure 3.10 Power Voltage curve for Gen 2 out- Peak Load (5 H)

The comparison between different power factor values has been analyzed. Changing the power factor from 0.9 to 0.8 changes the voltage values slightly. It does not have great impact on the system in this setup.

Table 3.16 Output data for fixed Q (starting pf 0.8- reactor 5 H)

| Solar Generator at BUS 6 | Reactor added at Bus 9 | Operating Mode of solar generator | Voltage at BUS 6 | Angle | Slack BUS | | Loss | |
|---|---|---|---|---|---|---|---|---|
| | | | | | MW | MVAR | MW | MVAR |
| 0 | 5 H | N/A | 1.05 | -10.33 | 222 | -57 | 3 | 131 |
| 50 | | lead | 1.02 | -5.48 | 171 | -40 | 1.5 | 136 |
| | | lag | 1.13 | -6.09 | 171 | -109 | 2 | 151 |
| 200 | | lead | 1.04 | 8.20 | 23 | -20 | 4 | 119 |
| | | lag | 1.13 | 6.18 | 23 | -98 | 4 | 139 |
| 400 | | lead | 1.02 | 27.03 | -159 | 43 | 20 | 131 |
| | | lag | 1.09 | 24.96 | -160 | 13 | 19 | 126 |
| 600 | | Lead/lag/unity | Does not converge | | | | | |

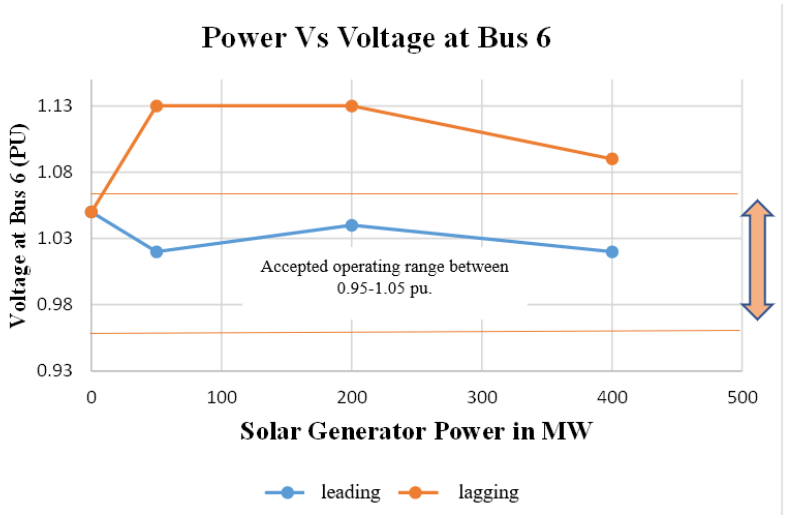


Figure 3.11 Power Voltage curve for Gen 2 out- Peak Load

### 3.3.2 Contingency Analysis (N-1 Gen 2 out- Min Load)

The same case for minimum load attached is described in this section. The load value was 30% as described in the previous sections. Generator 2 value of 163 MW was disconnected from the network and load flow analysis has been completed.

Table 3.17 Input data used for Gen 2 out min load

| Bus no | Bus Code | Voltage (pu) | Generation | | | Load | |
|---|---|---|---|---|---|---|---|
| | | | MW | MVAR | | MW | MVAR |
| | | | | Min | Max | | |
| 1 | PV | 1.04 | 10 | -5 | 5 | 0 | 0 |
| 2 | PV | 1.025 | ~~163~~ 0 | ~~-67~~ 0 | ~~67~~ 0 | 0 | 0 |
| 3 | PV | 1.025 | 85 | -40 | 40 | 0 | 0 |
| 4 | PQ | 1 | 0 | 0 | 0 | 0 | 0 |
| 5 | PQ | 1 | 0 | 0 | 0 | ~~125~~ 37 | 0 |
| 6 | PQ | 1 | 0 | 0 | 0 | ~~90~~ 27 | 0 |
| 7 | PQ | 1 | 0 | 0 | 0 | 0 | 0 |
| 8 | PQ | 1 | 0 | 0 | 0 | ~~100~~ 30 | 0 |
| 9 | PQ | 1 | 0 | 0 | 0 | 0 | 0 |

Reactor value 1 H was selected in this case. Because this reactor value can keep all base case bus voltage values within range. The power and voltage relation curve for this contingency analysis has been shown in Figure 3.12.

Table 3.18 Output data for fixed Q (starting pf 0.9- reactor 1 H)

| Solar Generator at BUS 6 | Reactor added at Bus 9 | Operating Mode of solar generator | Voltage at BUS 6 | Angle | Slack BUS | | Loss | |
|---|---|---|---|---|---|---|---|---|
| | | | | | MW | MVAR | MW | MVAR |
| 0 | 1 H | N/A | 1.04 | 1.34 | -2 | -30 | 2 | 135 |
| 200 | | lead | 1.00 | 21.06 | -192 | 46 | 11 | 88 |
| | | lag | 1.07 | 19.06 | -193 | 2 | 10 | 90 |
| 250 | | lead | 0.97 | 27.94 | -237 | 84 | 17 | 102 |
| | | lag | 1.05 | 24.19 | -239 | 30 | 15 | 102 |
| 400 | | Lead/lag | Does not converge | | | | | |

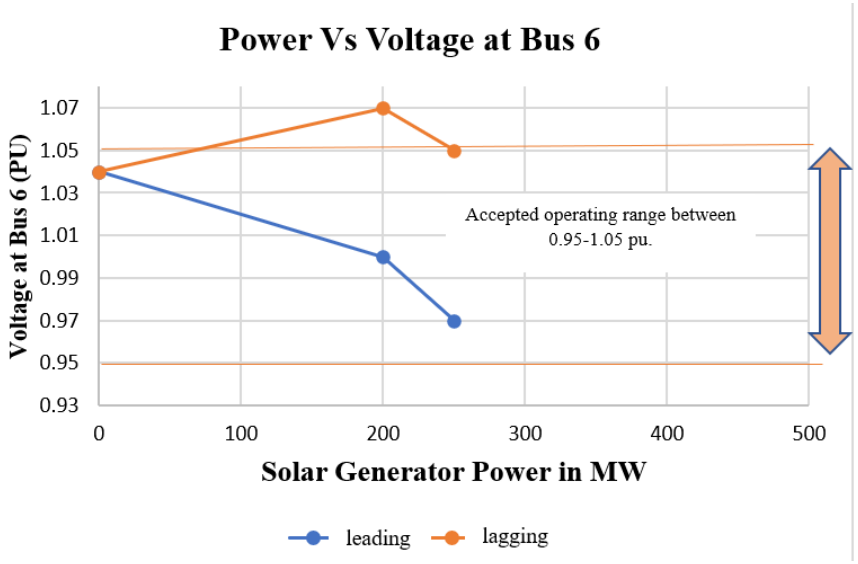


Figure 3.12 Power Voltage curve for Gen 2 out- Min Load (1 H)

If reactor is not connected, a 400 MW leading solar generator can be penetrated into this system setup having the following result in Table 3.19.

Table 3.19 Output data for fixed Q (starting pf 0.9- reactor 0 H)

| Solar Generator at BUS 6 | Reactor added at Bus 9 | Operating Mode of solar generator | Voltage at BUS 6 | Angle | Slack BUS | | Loss | |
|---|---|---|---|---|---|---|---|---|
| | | | | | MW | MVAR | MW | MVAR |
| 400 | 0 H | lead | 0.99 | 40.93 | -367 | 110 | 37 | 175 |
| | | lag | 1.05 | 38.60 | -370 | 81 | 34 | 170 |
| 600 | | Lead/lag | Does not converge | | | | | |

Table 3.20 Output data for power factor 0.8 (reactor 1 H)

| Solar Generator at BUS 6 | Reactor added at Bus 9 | Operating Mode of solar generator | Voltage at BUS 6 | Angle | Slack BUS | | Loss | |
|---|---|---|---|---|---|---|---|---|
| | | | | | MW | MVAR | MW | MVAR |
| 0 | 1 H | N/A | 1.04 | 1.19 | 6 | -30 | 1 | 135 |
| 50 | | lead | 1.00 | 6.41 | -48 | 3 | 2 | 120 |
| | | lag | 1.10 | 5.05 | -48 | -54 | 2.5 | 136 |
| 200 | | lead | 0.97 | 21.66 | -189 | 62 | 11 | 87 |
| | | lag | 1.09 | 18.34 | -191 | -12 | 10 | 90 |
| 400 | | lead | Does not converge | | | | | |
| | | lag | 0.76 | 61.22 | -337 | 318 | 63 | 342 |
| 600 | | Lead/lag/unity | Does not converge | | | | | |

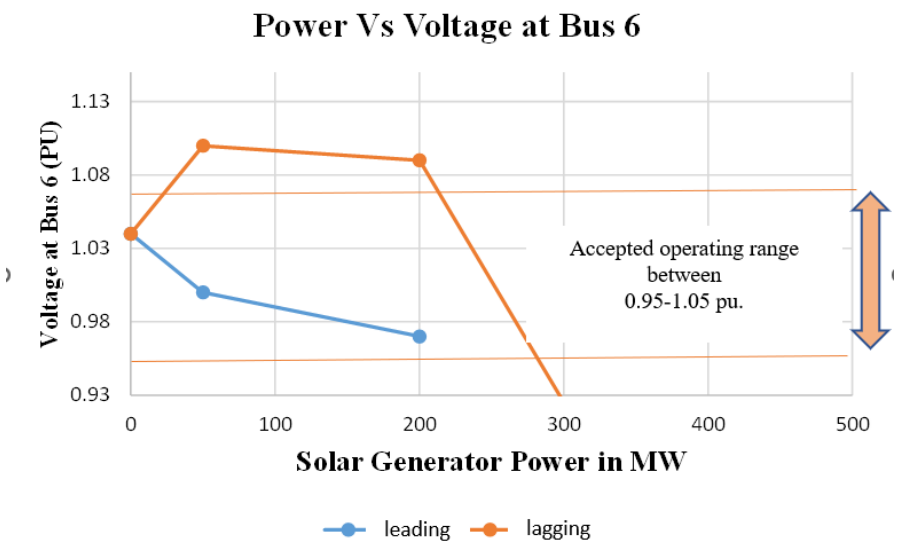


Figure 3.13 Power Voltage curve for Gen 2 out- Min Load (1 H)

### 3.4 Minimum and Maximum Load Profile Analysis

To compare the previous results for all cases together, this analysis of load profile has been done. Bus voltage values have been listed for peak load and minimum load cases separately and plotted in a single graph for comparison of three cases.

#### 3.4.1 Minimum Load Profile

Among the six case studies in this chapter, three cases consist of minimum load. The best values have been taken to consider this analysis. Bus 6 voltage values have been taken and those values are plotted against the increasing solar penetration level. AFI, Gen-3-out and Gen-2-out minimum load case have been observed and plotted in Figure 3.14. The values have been listed in Table 3.21.

Table 3.21 Minimum Load profile Data

| Solar Generator (MW) | All Facility Included | | Gen 3 out | | Gen 2 out | |
|---|---|---|---|---|---|---|
| | Voltage(pu) | Angle | Voltage(pu) | Angle | Voltage(pu) | Angle |
| 0 | 1.04 | 8.26 | 1.04 | 2.55 | 1.04 | 1.34 |
| 50 (lead) | - | - | 1.03 | 7.32 | - | - |
| 100 (lead) | 0.99 | 18.61 | - | - | - | - |
| 200 (lead) | 0.97 | 29.09 | 1.04 | 21.27 | 1.00 | 21.06 |
| 250 | - | - | - | - | 0.97 | 27.94 |
| 400 (lag) | 1.01 | 49.01 | 0.99 | 43.01 | - | - |
| 600 | - | - | - | - | - | - |

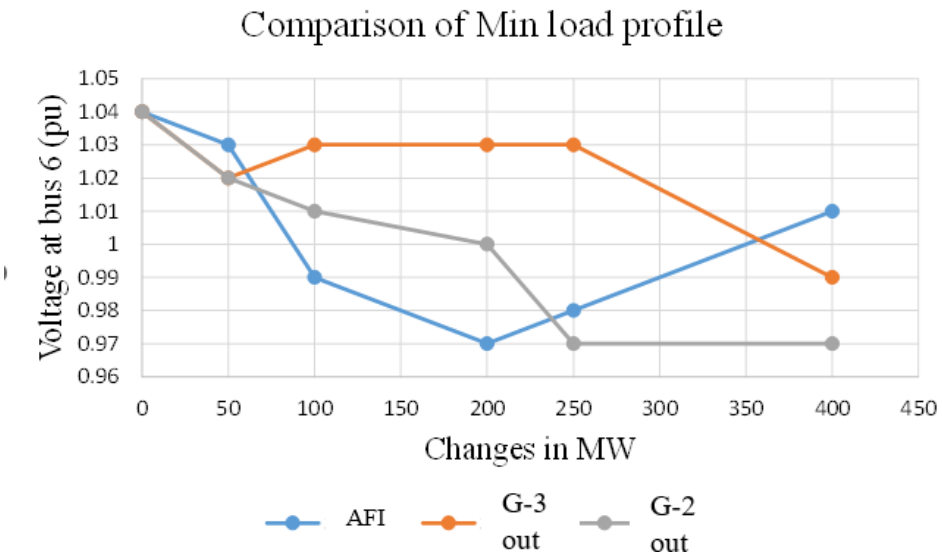


Figure 3.14 Minimum Load Profile

From Figure 3.14, all three case values are within range, but AFI has lower bus voltage values than Gen-3-out and Gen-2-out. When one generator is shut down from the network, there

is an imbalance, and the slack bus is going to balance the whole system. That is why contingency cases have more fluctuation compared to AFI.

### 3.4.2 Maximum Load Profile

As described in section 3.4.1, the same study has been conducted for maximum load case. The values listed in Table 3.22 and Figure 3.15 shows the graph for the maximum load case. The purpose of this graph is to compare all three maximum load cases.

Table 3.22 Maximum Load profile Data

| Solar Generator (MW) | All Facility Included | | Gen 3 out | | Gen 2 out | |
|---|---|---|---|---|---|---|
| | Voltage(pu) | Angle | Voltage(pu) | Angle | Voltage(pu) | Angle |
| 0 | 1.05 | -3.20 | 0.99 | -9.30 | 1.05 | -10.33 |
| 50 | 1.03 | 1.63 | 1.03 | -4.54 | 1.03 | -5.56 |
| 100 | 1.01 | 6.53 | 1.04 | 9.35 | - | - |
| 200 | 0.89 | 18.29 | - | - | - | - |
| 350 | 0.80 | 38.33 | - | - | 1.04 | 21.68 |
| 400 | | | 0.99 | 35.19 | 1.08 | 25.35 |

From Figure 3.14 and Figure 3.15, minimum load cases are more fluctuating and violating in terms of bus voltages. The reason behind this is that when loads at three buses are reduced by 30%, the network has more power to balance at an instant. Again, solar is injecting more power into the network with a reduced load, this causes overvoltage on the system for minimum load cases. The comparison graph shows it clearly.

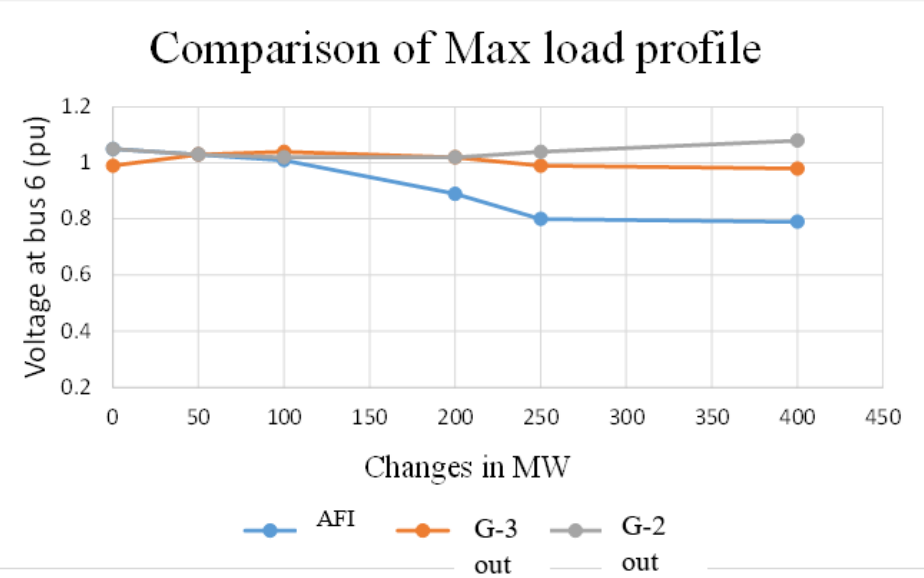


Figure 3.15 Maximum Load Profile

### 3.5 Comparison of load profile with loss

As shown in the table of previous sections, loss calculation has been done with increasing penetration of solar generation in the IEEE 9-bus system. The loss values have been assigned in the respective tables for each case. Both real and reactive power losses are listed in the tables. Here real power loss values have been considered and plotted.

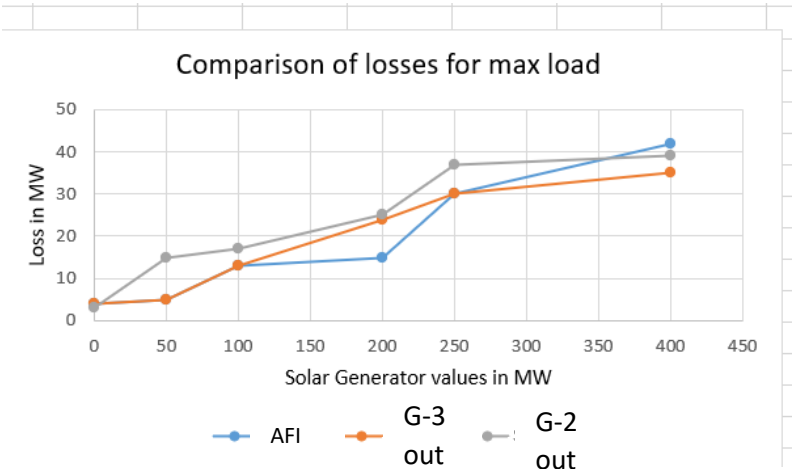


Figure 3.16 Loss Comparison for Peak Load

The comparison for minimum and maximum loss cases have been listed in Figures 3.16 and 3.17 respectively. In Figure 3.16, Real loss values have been plotted with respect to increasing solar penetration. The loss value for Gen-2-out case is maximum as the generator is located far away from the solar generator installed at bus 6. The solar generator installed cannot make up for the losses due to the distance of generator 2 from bus 6.

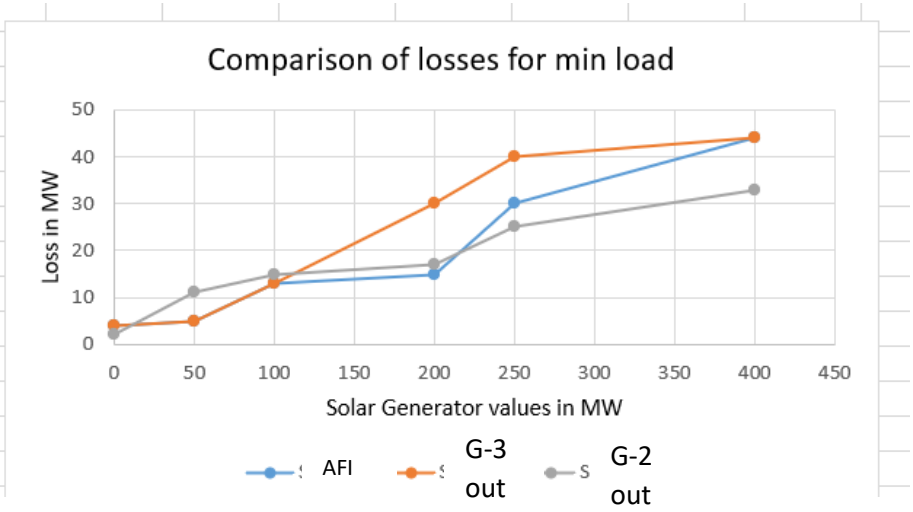


Figure 3.17 Loss Comparison for Min Load

In Figure 3.17, loss vs solar generation is plotted. Here the maximum loss value has been observed for Gen-3-out case. The loads have been reduced by 30% and the network faces more fluctuation in minimum cases. By comparing figures 3.16 and 3.17, it can be observed that the peak load case has less power loss than the minimum load case because of the location of solar generator and load sizes.

# CHAPTER 4
# CONCLUSIONS AND FUTURE WORK

In the present thesis, the IEEE 9-bus test case has been used to develop a methodology to study the voltage characteristics of a power system with solar penetration. This work has set the base for extending the analysis to the real New England power system.

One of the contributions of this thesis is the model and its values developed for simulations and the analysis of its results, as it will be available to future students conducting power system analysis with SKM. This model could potentially be included in the SKM library as an additional functionality of the toolbox, so that all its users can benefit from it, therefore contributing to the philosophy of open-source freeware as SKM.

The limitation of SKM software was one of the most challenging issues while conducting this research. Islanded microgrids cannot be analyzed with the same SKM setup. Also, transient analysis is not supported for the simulation of this particular model. Another version of SKM or ETAP can be used for transient analysis and islanded microgrid with solar penetration.

The voltage performance observed in Chapter 3 raises a question about overvoltage regulations in power systems. However, high-voltage regulation has not been paid much attention to. This thesis shows that there is a need for a deeper knowledge of power system overvoltage. To further enhance the research presented in this thesis, it may be beneficial to explore a more intricate model of voltage regulators. One of the goals of this thesis was to shed some light on the voltage and angle values of grid-connected microgrids. The simulations using this type of solar generator with grid connection show that further study is needed regarding its modeling, and in particular, the SKM model should be further validated for island cases. The analysis of the simulations

conducted in Chapter 3 shows that the interconnection between the solar generator and the rest of the power system plays a significant role in the effects on its voltage performance.

Chapter 3 has also shown the combined effect of changing solar penetration level with fixed reactive power and fixed power factor for grid connected systems. Therefore, analysis for the best-case and worst-case scenarios has been done. AFI min load case has been considered as the worst-case scenario as it consists of most of the violations. One contingency case is considered as best because it has all the voltage values within the acceptable range as described in chapter 3.

Regarding future work, the main goal should be to extend the present study to the real New England power grid. As a first step, a study using more detailed modeling of islanded microgrids for the six scenarios described in Chapter 3. For this work, it is recommended to make use of a bigger test case than the 39-bus system, as it would allow analyzing the behavior of solar farms in a bigger power system. In addition, large power system networks will require protection schemes for transmission lines such as relays or filters. Institutions such as NERC have thoroughly studied low-voltage-ride-through characteristics of solar panels and developed standards that utilities must follow to maintain stability in their systems.

Finally, the study on the influence of renewable sources at the point of interconnection could be expanded to consider offshore wind farms, given the distinctive characteristics of the connecting subsea cable and their recent increase in popularity. This study does not include transient operation mode which is a future work to do.

## REFERENCES


1. "The Status of Renewable Electricity Mandates in the States," Report by the Institute for Energy Research, 2011.

2. "ISO New England's Resource Mix," [Online].
   Available: http://www.isone.com/about/what-we-do/key-stats/resource-mix.

3. T. I. Rahman, M. Musavi, "Smart Grid and Micro Grid in the US: Distribution and Comparison", 2022 IEEE International Conference on Power Systems and Electrical Technology, October 13-15, 2022.

4. "Center for Climate and Energy Solutions", C2ES website [Online]. Available: https://www.c2es.org/content/microgrids/#:~:text=Microgrids%20provide%20less%20than%200.2,York%2C%20Oklahoma%2C%20and%20Texas

5. "Department of Energy Releases New Tool Tracking Microgrid Installations in the United States", Office of Energy Efficiency & Renewable Energy webpage, 2022 [Online]. Available: https://www.energy.gov/eere/amo/articles/department-energy-releases-new-tool-tracking-microgrid-installations-united

6. "US Energy Information Administration (EIA), Independent Statistics and Analysis, 2020", [Online]. Available:https://www.eia.gov/tools/faqs/faq.php?id=65&t=2

7. L. Badesa, "Impact of Wind Generation on Dynamic Voltage Characteristics of Power Systems", MS Dissertation, University of Maine, May 2016.

8. Y. Chi, Y. Liu, W. Wang and H. Dai, "Voltage Stability Analysis of Wind Farm Integration into Transmission Network," Proceedings of the International Conference on Power System Technology, 2006.

9. H. T. Le and S. Santoso, "Analysis of Voltage Stability and Optimal Wind Power Penetration Limits for a Non-radial Network with an Energy Storage System," Proceeding of the IEEE PES General Meeting, 2007.

10. A. Teninge, D. Roye, S. Bacha and J. Duval, "Low voltage ride-through capabilities of wind plant combining different turbine technologies," Proceeding of the European Conference on Power Electronics and Applications, 2009.

11. "U.S. Department of Energy (DOE), EERE, Renewable Energy", Office of Energy Efficiency & Renewable Energy, [Online]. Available: https://www.energy.gov/eere/renewable-energy

12. T. Drake, J. Matson, "Designing Microgrids for Efficiency and Resiliency", July 30, 2021, Sustainable Solutions, [Online]. Available: https://www.mtu-solutions.com/na/en/technical-articles/2021/designing-microgrids-for-efficiency-and-

resiliency.html#:~:text=By%20utilizing%20renewable%20energy%20sources,to%20conventional%20power%20generation%20techniques

13. K. S. Shetye, "Validation of Power System Transient Stability Results," MS Thesis, University of Illinois at Urbana-Champaign, 2011.

14. J. J. Grainger and W. D. Stevenson, "Chapter 8: The Impedance Model and Network Calculations," in Power System Analysis, 1st Edition, McGraw-Hill, 1994, pp. 287-289.

15. J. D. Glover, M. S. Sarma and T. Overbye, "Chapter 4: Transmission Line Parameters," in Power System Analysis and Design, 5th Edition, Cenage Learning, 2012.

16. H. Saadat, "Power System Analysis," in Chapter 2: Basic Principles, 3rd Edition, PSA Publishing, 2010, pp. 66-67.

17. H. Saadat, "Chapter 1: The Power System and Electric Power Generation," in Power System Analysis, 3rd edition, PSA Publishing, 2010, pp. 26-29.

18. "Alternative Energy Tutorials: Syncrhonous Generator," [Online]. Available:http://www.alternative-energy-tutorials.com/wind-energy/synchronous-generator.html.

19. M. A. H. Ahim, “Power system analysis using SKM power tools”, 7th Brunei International Conference on Engineering and Technology 2018 (BICET 2018).

20. T. Ackermann, R. Kuwahata, “Lessons Learned from International Wind Integration Studies”, Energynautics, November 2011.

21. Power*Tools for Windows Version 8.0 Enhancements, System Analysis Icc, Available: https://www.skm.com/download/ptw_v8.0_enhancement_list.pdf

22. Dapper Studies, SKM Analysis Inc. Available: https://www.skm.com/Dapper.html

23. H. Saadat, "Chapter 3: Generator and Transformer Models; the Per-Unit System," in Power System Analysis, 3rd Edition, PSA Publishing, 2010, pp. 88-89.

24. F. Milano, Documentation for Power System Analysis Toolbox version 2.1.6, 2011.

25. H. Saadat, "Chapter 11: Stability," in Power System Analysis, 3rd Edition, PSA Publishing, 2010, pp. 500-503.

26. A.S. Saidi, M. E. Mudwah, K. B. Kilani, “Assessment of PV Systems Stability under Temperature Variation”, The 9th International Renewable Energy Congress (IREC 2018).

27. A. Kaur, “Load Flow Studies”, Department of Electrical Engineering, GNDEC, Ludhiana.Available:https://www.powershow.com/view0/7cc643-ZTA1M/Load_Flow_Studies_powerpoint_ppt_presentation

28. L. Mones, “A Gentle Introduction to Power Flow”, Invenia, 04 Dec 2020. Available: https://invenia.github.io/blog/2020/12/04/pfintro/#:~:text=Based%20on%20Kirchhoff's%20current%20law,V%20i%20T%20i%20j%20.

29. Load Flow Analysis (LFA), Power Research and Development Consultants Pvt. Ltd,PSCT, Protection Analytic Tool. Available: https://erpc.gov.in/wp-content/uploads/2016/09/1.-Load-Flow-Analysis-User-Manual.pdf

30. J. G. Slootweg, "Wind Power Modelling and Impact on Power System Dynamics," PhD Dissertation, Delft University of Technology (Netherlands), 2003.

31. O. A. Afolabi, W. Ali, P. Cofie, J. Fuller, “Analysis of the Load Flow Problem in Power System Planning Studies”, Energy and Power Engineering 07(10):509-523, January 2015.

## BIOGRAPHY OF THE AUTHOR

Tasnim Ikra Rahman was born in Khulna, Bangladesh on September 10, 1994. She completed her high school from Viqarunnisa Noon School and College in 2011. She attended Military Institute of Science and Technology, Bangladesh and graduated with a Bachelor of Science in Electrical, Electronics and Communication Engineering in 2016. She received the Dean's Award for Academic Excellence during her undergraduate program. She completed her MS degree with a major in Renewable Energy Technology in 2019 from the University of Dhaka. Tasnim is a candidate for the Master of Science degree in Electrical Engineering from the University of Maine in August 2023.